# Late Ordovician Glaciation Initiated by Early Land Plant Evolution and Punctuated by Greenhouse Mass Extinctions

*Gregory J. Retallack**

*Department of Geological Sciences, University of Oregon, Eugene, Oregon 97403-1272, USA*

**ABSTRACT**

Late Ordovician (Hirnantian) glaciation, indicated by periglacial paleosols, tillites, and glacial pavements in Saharan Africa, has been attributed to advances in weathering and carbon sequestration due to evolution of early land plants, in the same way that Devonian-Permian glaciation has been attributed to evolution of forests and Quaternary glaciations to evolution of grasslands. Two problems for carbon cycle explanations of this glaciation are an Hirnantian $CO_2$ greenhouse estimated at 4035 ppmv from mass balance models and possibly related Hirnantian mass extinctions. This estimate of high $CO_2$ is a 10-m.yr. average, here evaluated against high-resolution sequences of paleosols that give estimates not only of $CO_2$ but also of paleoclimate and vegetation through the Late Ordovician. Katian paleosols of the eastern United States show increases in depth and in degree of carbon consumption and storage comparable with those preceding glaciation of the Devonian-Permian and Quaternary. Early thalloid land plants with rhizoids may have drawn down atmospheric $CO_2$ to only 166 ± 83 ppmv during the Hirnantian, as estimated here from a pedogenic $CO_2$ paleobarometer. Ordovician paleosols also reveal a short-term greenhouse spike to as much as 4670 ppmv immediately before Hirnantian glaciation. This greenhouse spike may be due to thermogenic methane release from a large igneous province and is comparable with greenhouse spikes during other mass extinctions, such as those of the Late Permian and Late Jurassic.

**Online enhancements:** supplementary tables.

## Introduction

The Late Ordovician (Hirnantian) glaciation is well documented from periglacial paleosols, tillites, and glacial pavements in Saharan Africa (Le Heron and Craig 2008; Finnegan et al. 2011), but it has been a paradox for carbon cycle models because it occurred at a time of a $CO_2$ greenhouse (Yapp and Poths 1992; Berner 2006) and attendant mass extinctions (Fan et al. 2009; Harper et al. 2014). The Late Ordovician was also a time of evolutionary radiation of early land plants, with consequences for terrestrial weathering that may have ushered in the ice age (Retallack 2000, 2003; Lenton et al. 2012). This study attempts to reconcile apparent contradictions in paleoclimatic and biotic history of the Late Ordovician by reexamining paleosol records from Pennsylvania (Retallack and Feakes 1987; Feakes and Retallack 1988) and Tennessee (Driese and Foreman 1991, 1992) and by comparing paleosols from Wisconsin (Yapp and Poths 1992, 1993, 1994), Nova Scotia (Feakes et al. 1989; Jutras et al. 2009), and Australia (Retallack 2009*a*, 2009*b*). Paleosols have unique advantages for such a study because the same paleosol can furnish estimates of paleoprecipitation (Retallack 2005), paleotemperature (Óskarsson et al. 2009), paleoproductivity, and atmospheric $CO_2$ (Breecker and Retallack 2014). In addition, long paleosol sequences are now available from the Cambrian through Devonian (Retallack 2008, 2009*a*, 2009*b*; Retallack and Huang 2011), with temporal resolution equal to marine carbonate curves of $\delta^{13}C$, $\delta^{18}O$, and $^{86}Sr/^{87}Sr$ (Veizer et al. 1999; Prokoph et al. 2008). Thus, both short-term (<1 m.yr.) perturbations like mass extinctions and long-term (>10 m.yr.) trends like paleoclimatic cooling can be compared both on land and at sea.

Hypotheses for glaciations in deep time fall into three general categories: (1) volcanic-tectonic, (2) ocean-

Manuscript received May 4, 2015; accepted August 14, 2015; electronically published November 17, 2015.

* E-mail: gregr@uoregon.edu.

[The Journal of Geology, 2015, volume 123, p. 509–538]  0022-1376/2015/12306-0002$15.00. DOI:10.1086/683663

atmosphere circulation, and (3) biotic. Uplift of the Himalaya, for example, has been thought to have increased Cenozoic chemical weathering and carbon sequestration to draw down a greenhouse atmosphere (Raymo and Ruddiman 1992). Ocean circulation changes, such as initiation of the Antarctic Circumpolar Current, have also been implicated as causes of Cenozoic glaciation (Kennett 1982). A biotic hypothesis for inducing Cenozoic glaciation is the evolution of grasslands with Mollisols, which are moist, organic-rich soils of high albedo vegetation (Retallack 2003, 2013*a*). Similarly, Devonian to Permian glaciation can be considered the result of Acadian-Hercynian mountain uplift (Raymo 1991), Iapetan ocean enclosure (Crowell 1978), or evolution of forests with deep clayey (Alfisol and Ultisol) and peaty (Histosol) soils (Berner 1997; Retallack and Huang 2011). Hirnantian glaciation has been attributed to Taconic mountain uplift (Kump et al. 1999), amalgamating and expanded microcontinents (Saltzman and Young 2004), or evolution of early land plants increasing the depth and degree of weathering on land (Retallack 2000, 2003; Lenton et al. 2012).

Among the various causes for Late Ordovician mass extinction (Harper et al. 2014), Hirnantian glaciation has been a leading suspect (Brenchley et al. 1995), but extinction precedes glaciation when detailed stratigraphic records are considered (Lefebvre et al. 2010; Ghienne et al. 2014). Three additional hypotheses for mass extinction will also be considered here: (1) methane and carbon dioxide from unusually large volcanic eruptions, (2) nitric and sulfuric acid from asteroid or other extraterrestrial impact, and (3) sulfides from oceanic stagnation. A mechanism of thermogenic methane release by feeder dikes of large igneous provinces has been proposed for Late Permian mass extinctions (Retallack and Jahren 2008) and has also been inferred for other mass extinctions (Keller 2011; Bond and Wignall 2014). Black pyritic shales with biomarker evidence for atmospheric release of sulfides and sulfuric acid are known for Late Permian (Grice et al. 2005; Bond and Wignall 2014; Sephton et al. 2015) and Late Triassic (van de Schootbrugge et al. 2013) mass extinctions. Black shales and other evidence of anoxia are also known from the Hirnantian (Armstrong et al. 2009*a*; Fan et al. 2009; Hammarlund et al. 2012). Asteroid impact and attendant interruption of photosynthesis by dust clouds and acid rain has been demonstrated for Late Cretaceous mass extinction (Alvarez et al. 1995; Retallack 2004), but evidence of impact at other mass extinctions is not compelling (Retallack et al.1998; Becker et al. 2004). These various hypotheses for glaciation and mass extinction are testable by paleosol evidence of changes in paleoclimate and atmospheric $CO_2$.

## Material and Methods

The most informative sections of paleosols in the Juniata Formation in Pennsylvania (fig. 1*A*) were roadcuts 4 km east of Potters Mills (Centre County) on US Highway 322 (40.768004°N, 77.398268°W), 1 km east of Reedsville (Mifflin County) on Old US Highway 322 (40.655731°N, 77.59686°W), and 1 km east of Loysburg (Bedford County) on State Highway 35 along Yellow Creek (40.159172°N, 78.370733°W). These outcrops were fresh in 1983 when first examined but are now becoming overgrown with crown vetch (*Coronilla varia*) sown by the state highway department. Five additional sites in Pennsylvania documented by Retallack (1985) now show only small amounts of sandstone and no paleosols. Also reexamined for this study in 2001 and 2012 is a section in Tennessee (fig. 1*B*) studied by Driese and Foreman (1991, 1992) opposite the cafe and viewpoint at

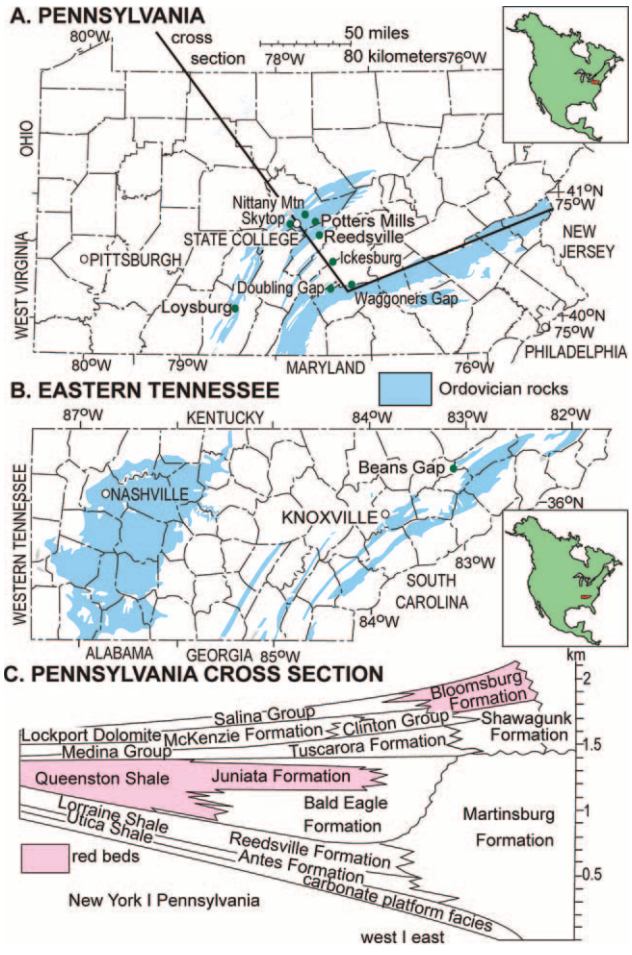


**Figure 1.** Ordovician paleosol localities and outcrops of Pennsylvania (*A*) and Tennessee (*B*) and a geological cross section of Pennsylvania (from Thompson 1999; *C*).

Beans Gap (Grainger County) on US Highway 25E (36.351261°N, 83.397705°W).

A variety of paleoenvironmentally significant measures were taken in the field: Munsell hue, nodule size, depth to calcareous nodules, thickness of paleosol with nodules, and depth of bioturbation (Retallack 2005). Carbonate in the Juniata Formation is partly dolomitic (Retallack 1993) and weakly reactive to acid but is distinctive in nodular form and light color, so it was estimated as volume percent in outcrop using a relative abundance card (Terry and Chilingar 1955). Separate rock and carbonate samples were collected from representative beds for laboratory analyses: major and trace element geochemical analysis by x-ray fluorescence, ferrous iron by potassium dichromate titration (by ALS Chemex, Vancouver, British Columbia), and bulk density determined from the weight suspended in air and then water of a paraffin-coated clod. Petrographic thin sections were cut from the same samples, and 500 points were counted using a Swift automated point counter to determine grain-size distribution and mineral composition (see tables S1–S3, available online).

Also a part of this work was assembly of databases on late Cambrian to early Devonian paleosol depth to carbonate (Retallack 2008, 2009*a*, 2009*b*; Retallack and Huang 2011) and recalibration of marine carbonate isotopic data from old time scales used by Veizer et al. (1999) and Prokoph et al. (2008) to current understanding of numerical age of geological stages (Gradstein et al. 2012).

## Geological Setting of Appalachian Ordovician Paleosols

***Stratigraphy.*** The Juniata Formation is red siltstone and sandstone (figs. 1*A*, 1*B*, 2*A*–2*C*) widespread in the eastern Valley and Ridge Province of Pennsylvania, Virginia, West Virginia, and Tennessee (Thompson 1970*a*, 1970*b*, 1999; Driese and Foreman 1991, 1992). To the east, the Juniata Formation conformably overlies folded gray Martinsburg Formation (fig. 1*C*), which is evidence that it was a clastic wedge from Taconic mountain uplift (Hatcher et al. 1989). In central Pennsylvania, Virginia, and West Virginia, Juniata Formation conformably overlies red and green-gray sandstones and conglomerates of the Bald Eagle (fig. 1*C*) or Oswego Formation, which in turn conformably overlie gray shale and sandstone of the Reedsville Formation (Schuchert 1916). To the west, the Juniata Formation passes laterally into red Queenston Shale of New York (Dennison 1976) and red shale and dolostone of the Sequatchie Formation of Virginia, Tennessee, Georgia, and Alabama (Thompson 1970*b*). The Juniata Formation is abruptly overlain by quartz sandstones of the Tuscarora Formation in Pennsylvania (Schuchert 1916; Thompson 1999) and by the Clinch Sandstone in Virginia, West Virginia, Tennessee, Georgia, and Alabama (Driese and Foreman 1991, 1992). Although there is no angular discordance, this and other contacts within the Tuscarora and Clinch Sandstones have been considered disconformable (Dorsch et al. 1994).

***Geological Age.*** The precise age of the Late Ordovician Juniata Formation has been uncertain without age-diagnostic fossils but is constrained by marine rocks above and below (fig. 3*A*). The underlying Bald Eagle Formation has a distinctive fauna of large rhynchonellid brachiopods (*Orthorhynchula linneyi*) and bivalves (*Ambonychia* sp. indet.), of Richmondian (late Katian) age (Schuchert 1916). At Cumberland Gap, Tennessee, 70 m of Sequatchie Formation with late Katian marine brachiopods is considered laterally equivalent to the lower Juniata Formation (Thompson 1970*b*). The overlying Tuscarora and Clinch Sandstones have a marine trace fossil assemblage of uncertain geological age: *Arthrophycus alleghaniensis*, *Skolithos verticalis*, *Daedalus archimedes*, *Cruziana*, *Rusophycus*, *Planolites*, and *Monocraterion* (Butts 1940; Cotter 1983). The Tuscarora Formation of Pennsylvania also contains cryptospores like *Velatitetras rugosa* with a range of Sandbian–Rhuddanian (Johnson 1985; Vecoli et al. 2011), thus indicating that the Tuscarora Formation began accumulating during the earliest Silurian. Another point of correlation for the Clinch Sandstone is the Thorn Hill K-Bentonite Complex 30–480 m above the Juniata Formation at Beans Gap and elsewhere in Tennessee and correlated into fossiliferous sections near Cincinnati of Aeronian or mid–Early Silurian age (Manzo et al. 2002). Above that again the Castanea Sandstone and Rose Hill Formation, near Reedsville, Pennsylvania, have brachiopods, trilobites, and ostracods of Telychian or late Early Silurian age (Schuchert 1916).

Traditionally, the Ordovician-Silurian boundary has been placed within a hiatus between the Juniata and Tuscarora Formations or a hiatus within the Tuscarora Formation (Dorsch et al. 1994), comparable with the Martinsburg-Shawangunk hiatus to the east (fig. 1*C*). However, the Juniata Formation, like the latest Ordovician elsewhere, is entirely normally magnetized (Trench et al. 1991) and fails to show reversals found in the earliest Silurian Red Mountain Formation, equivalent to the Tuscarora Formation (Trench et al. 1991), thus supporting a Late Ordovician Juniata Formation and an Early Silurian Tuscarora Formation. Palynological (Johnson 1985; Vecoli et al. 2011) and tephrostratigraphic (Manzo et al. 2002) dating of the Tuscarora and Clinch Sandstones now indicate that little is missing from the

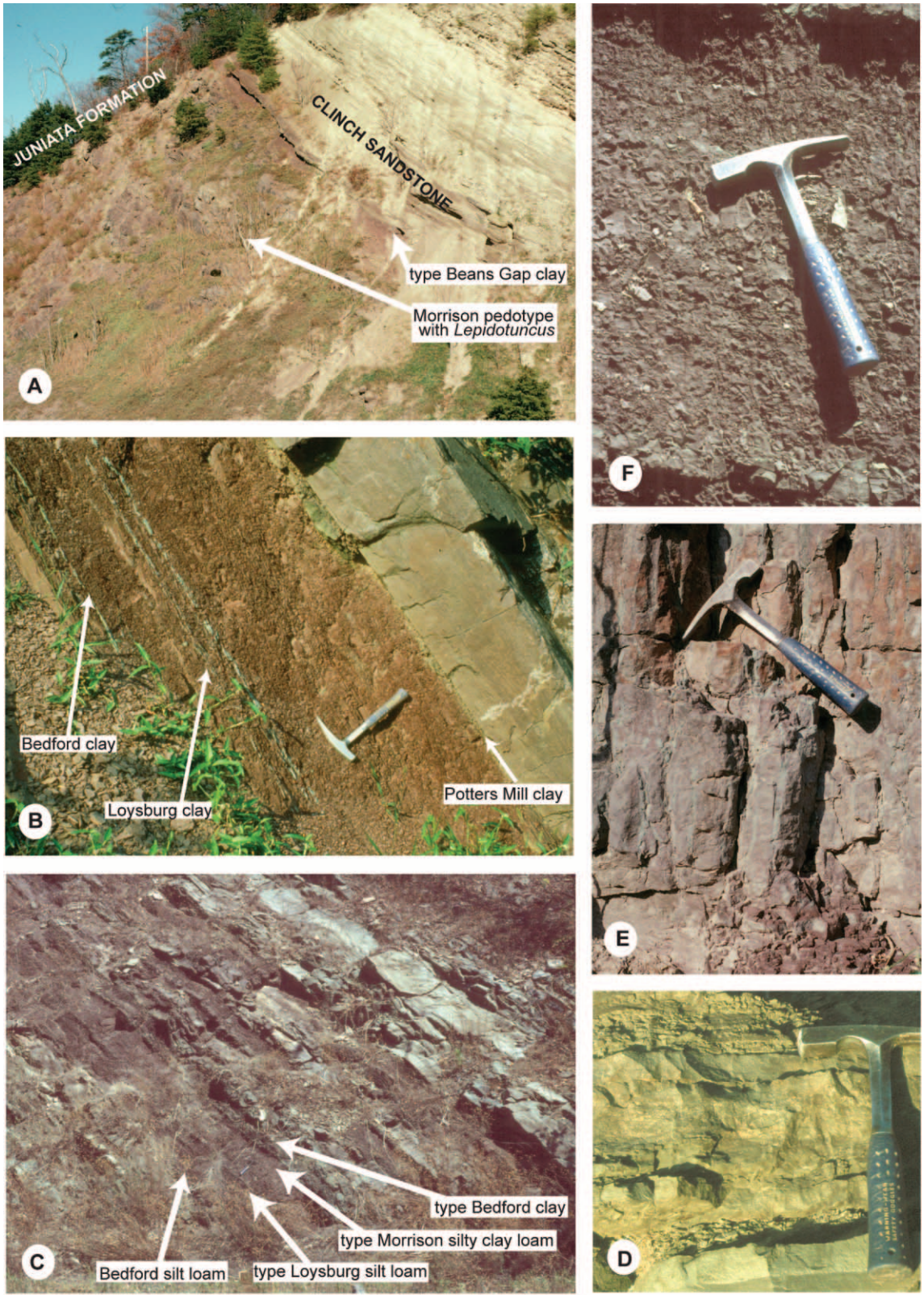


**Figure 2.** Ordovician paleosols in the field. *A*, Red clayey paleosols of the Juniata Formation overlain by white Clinch Sandstone in Beans Gap, Tennessee (exposed section is 35 m thick). *B*, Red clayey paleosols in the lower Juniata Formation near Reedsville, Pennsylvania (hammer shown for scale). *C*, Red clayey paleosols in the Bald Eagle Formation near Loysburg, Pennsylvania (hammer shown for scale on Loysburg pedotype). *D*, Type Tussey sandy clay loam paleosol at Loysburg with burrows of *Skolithos* (hammer shown for scale). *E*, Bedford pedotype paleosol with prototaxaleans in overlying sandstone at Beans Gap (hammer shown for scale). *F*, Type Morrison silty clay loam paleosol with fine blocky peds and *Scoyenia beerboweri* burrow at Loysburg (hammer shown for scale).

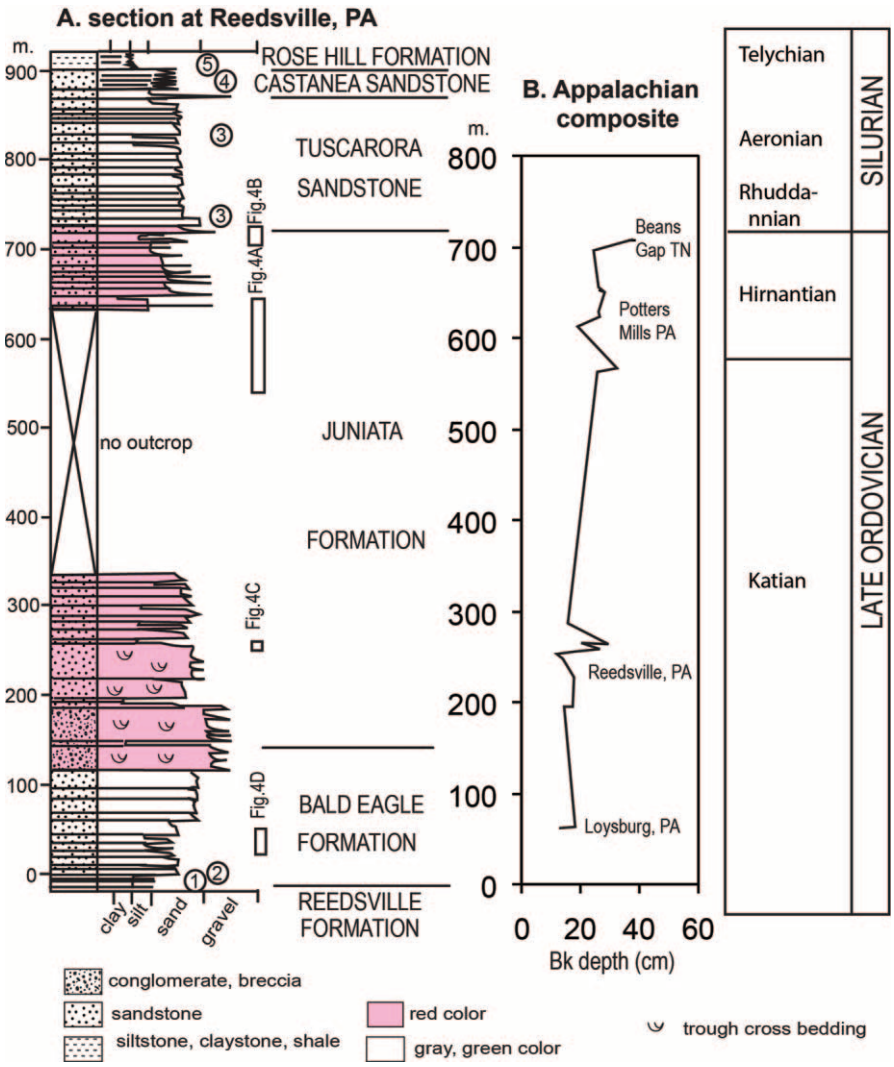


**Figure 3.** Stratigraphic levels and correlations of studied paleosols. *A*, Stratigraphic section near Reedsville, Pennsylvania (after Schuchert 1916; Horowitz 1965; Thompson 1968), and relative stratigraphic position of detailed sections (fig. 4). *B*, Depth to carbonate nodules (Bk horizon) in paleosols of all Appalachian sections examined.

earliest Silurian. Finally, correlation of global sea level inferred from cumulative aggradation plots and gamma ray logs of the Juniata Formation has revealed that the upper Juniata Formation is Hirnantian (Diecchio and Broderson 1994; Diecchio 1995) and thus correlative with global marine regression and glaciation in Saharan Africa (Le Heron and Craig 2008; Ghienne et al. 2014).

***Burial Alteration.*** The Juniata Formation and associated formations have been folded about northeast-southwest strike ridges (fig. 1*A*, 1*B*) that characterize the Appalachian Valley and Ridge province (Hatcher et al. 1989). Trioctahedral chlorite and dioctahedral illite in the Juniata Formation are evidence of metamorphism to lower greenschist facies (Thompson 1970*a*). Alteration of conodonts (CAI 4) in Ordovician limestones of central Pennsylvania is evidence of burial temperatures of 160°–210°C and burial depths of 4.6–6.6 km (Epstein et al. 1977). Local sulfide mineralization in the Bald Eagle Formation at Skytop includes quartz veins with fluid inclusion temperatures of 140°–375°C (McWilliams et al. 2006), but such locally high-temperature alteration was not seen at other localities examined for this work. Burial compaction to 70%–75% of the original volume of the paleosols in the Juniata Formation can be calculated using a standard compaction formula for calcareous soils (eq. [1] for Aridisols of Sheldon and Retallack 2001) to obtain the original thickness of soil ($B_s$ [cm]) from the thickness of paleosol ($B_p$

[cm]) for a known burial depth ($K$ [km]) of 4.6–6.6 km, as follows:

$$B_s = \frac{B_p}{-0.62/[(0.38/e^{0.17K}) - 1]}. \quad (1)$$

The red color of the Juniata Formation is from hematite of diagenetic origin (Thompson 1970*a*), recrystallized during early burial from goethite and other iron minerals during soil formation (Retallack 1985). Gray-green mottles also are ubiquitous in the surfaces of the paleosols (fig. 5) and, like comparable features in Cambrian (Retallack 2008) and Triassic (Retallack 1997) paleosols, may have been created by burial gleization of organic matter in original surface horizons. Early burial gleization is confirmed by magnetic susceptibility correlation with iron content due to open system alteration in mottles of the Potters Mills clay paleosol (Retallack et al. 2003).

## Paleosols and Associated Fossils

Sparsely fossiliferous red beds of the Juniata Formation have been considered nonmarine (Schuchert 1916), and their paleochannel form and sedimentary structures have been compared with those of braided streams (Cotter 1978, 1983; Davies and Gibling 2010). While acknowledging that there are no marine sedimentary structures or body fossils in the Juniata Formation, Davies et al. (2010, 2011) take the iconoclastic view that the Juniata Formation was marine because it is more clayey and rich in trace fossils than usual for a pre-Devonian fluvial formation. This view has been challenged elsewhere (Retallack et al. 2011*a*), and the following paragraphs detail further evidence for paleosols and terrestrial plants and animals in the Juniata Formation.

***Field and Petrographic Evidence of Paleosols.*** Paleosols are recognized by a trinity of (1) root traces, (2) soil horizons, and (3) soil structures (Retallack 2001*b*). True roots had not evolved by the Ordovician (Retallack 2000), but there are beds with irregular strata-transgressive tubular features that appear to be burrows and early land plants (figs. 5–7). Many beds in the Juniata Formation have the sharp top and gradational lower alteration characteristic of soil horizons (figs. 2*A*–2*C*, 5, 6). These truncated tops are strongly ferruginized and clayey and grade down into a subsurface zone of carbonate nodules (fig. 2*B*, 2*F*), like A-Bk-C profiles of paleosols, rather than bioturbated marine beds. Soil structure in sedimentary rock is often characterized as massive, featureless, and nondescript because it develops at the expense of familiar sedimentary structures, such as ripple marks, planar bedding, and cross-bedding. Sedimentary structures in the Juniata Formation have been obscured by a variety of distinctive soil features, including crack networks (peds and cutans; fig. 2*F*), bowl slickensides (stress argillans; Gray and Nickelsen 1989; Driese and Foreman 1992), clay skins (illuviation argillans; fig. 8*E*), expansion cracks (silans; fig. 8*D*), elongate drab reduction spots (gleyans; figs. 2*E*, 7*F*), and replacive dolomite and calcite nodules (caliche; figs. 7*C*, 8*C*). Petrographic thin sections show gradation between laminated argillasepic fabrics of sediments (fig. 8*D*) and massive mosepic porphyroskelic fabrics of soils (fig. 8*E*). Also comparable with soils is micritic carbonate intimately associated with burrows and sparry calcite tubes after plant remains (fig. 8*C*).

Distinctive kinds of Ordovician paleosols have already been named Potters Mills, Faust Flat (Feakes and Retallack 1988), Powell Mountain, and Beans Gap pedotypes (Driese and Foreman 1991), and this terminology is here amplified to eight pedotypes in the Juniata and Bald Eagle Formations (figs. 5, 6; tables 1, 2). Pedotypes are defined on the basis of field differences, such as clayeyness and color. Although named for its type locality (figs. 4*A*, 5, 6), the Potters Mills pedotype represents a specific kind of paleosol, which was also found at Beans Gap (fig. 4*B*) and Reedsville (fig. 4*C*). The Beans Gap and Powell Mountain pedotypes, in contrast, were seen only at these locations in Tennessee (Driese and Foreman 1991), at stratigraphic levels regarded here and by Diecchio (1995) as part of the basal Silurian marine transgression (fig. 3).

Each pedotype is based on a type profile, sampled in detail for petrographic and geochemical study to test the hypothesis that it is a paleosol (figs. 5, 6; for comparable data on Beans Gap and Powell Mountain pedotypes, see Driese and Foreman 1991). These additional data also allow identification of pedotypes within classifications of modern soils (table 1), such as the paleosol classification of Mack et al. (1993), the old (Stace et al. 1968) and new (Isbell 1998) Australian classifications, the world map of soils of the Food and Agriculture Organization (1974), and the soil taxonomy of the Soil Survey Staff (2010) of the US National Resources Conservation Service. Petrographic analysis has confirmed that these Ordovician paleosols all lack argillic horizons (illuvial clay-enriched horizons of Soil Survey Staff 2010), despite their clay skins, bioturbation, and thickness (figs. 2*F*, 5, 6) comparable with those of Argillisols (Mack et al. 1993), Podzols (Stace et al. 1968), Chromosols (Isbell 1998), Luvisols (Food and Agriculture Organization 1974), and Alfisols (Soil Survey Staff 2010).

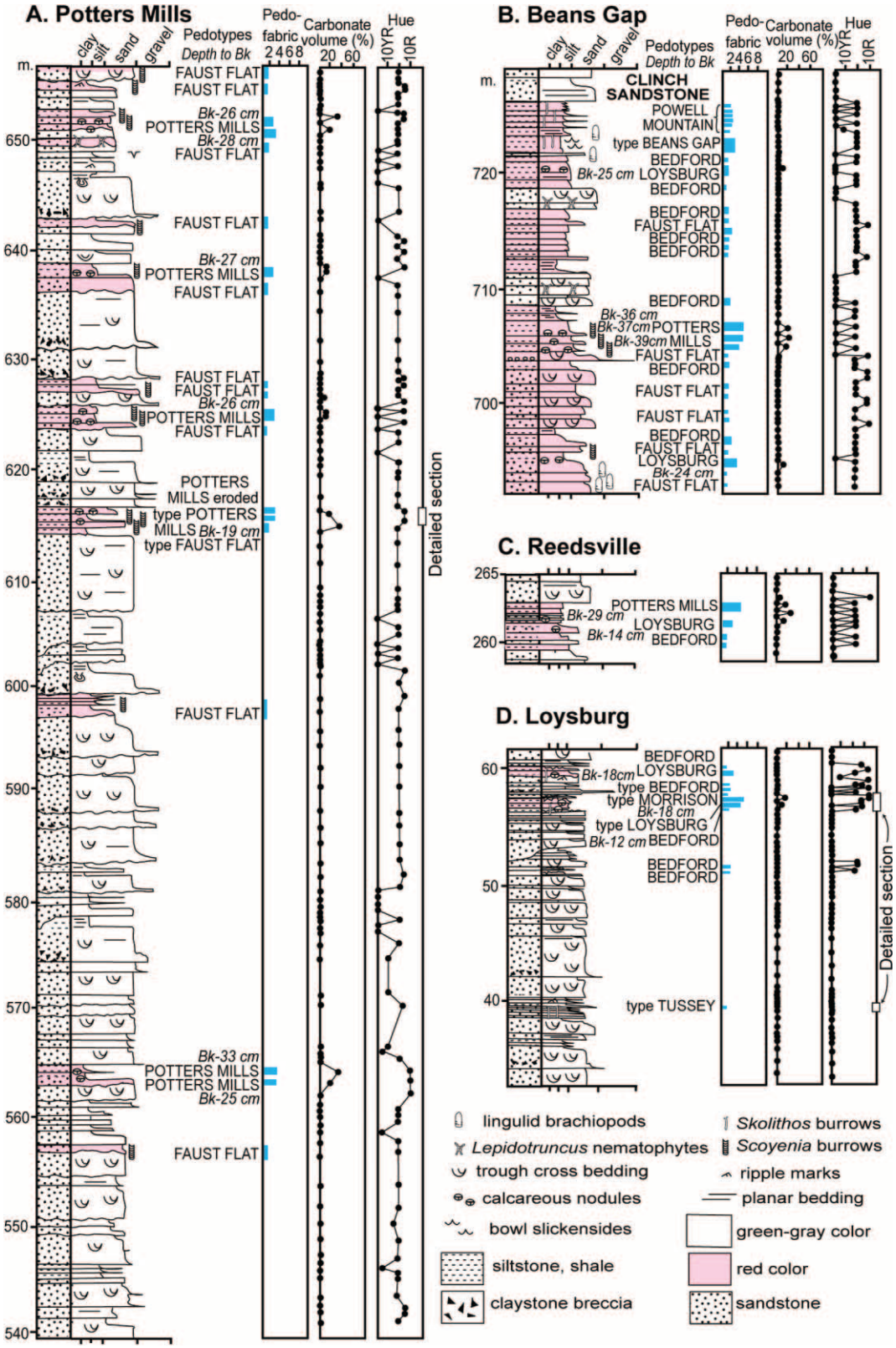


**Figure 4.** Detailed measured sections of Ordovician paleosols in Pennsylvania (*A*, *C*, *D*) and Tennessee (*B*). Columns by graphical log show paleosol development (from Retallack 2001*b*), volume percent carbonate nodules (estimated from the field card of Terry and Chilingar 1955), and Munsell hue.

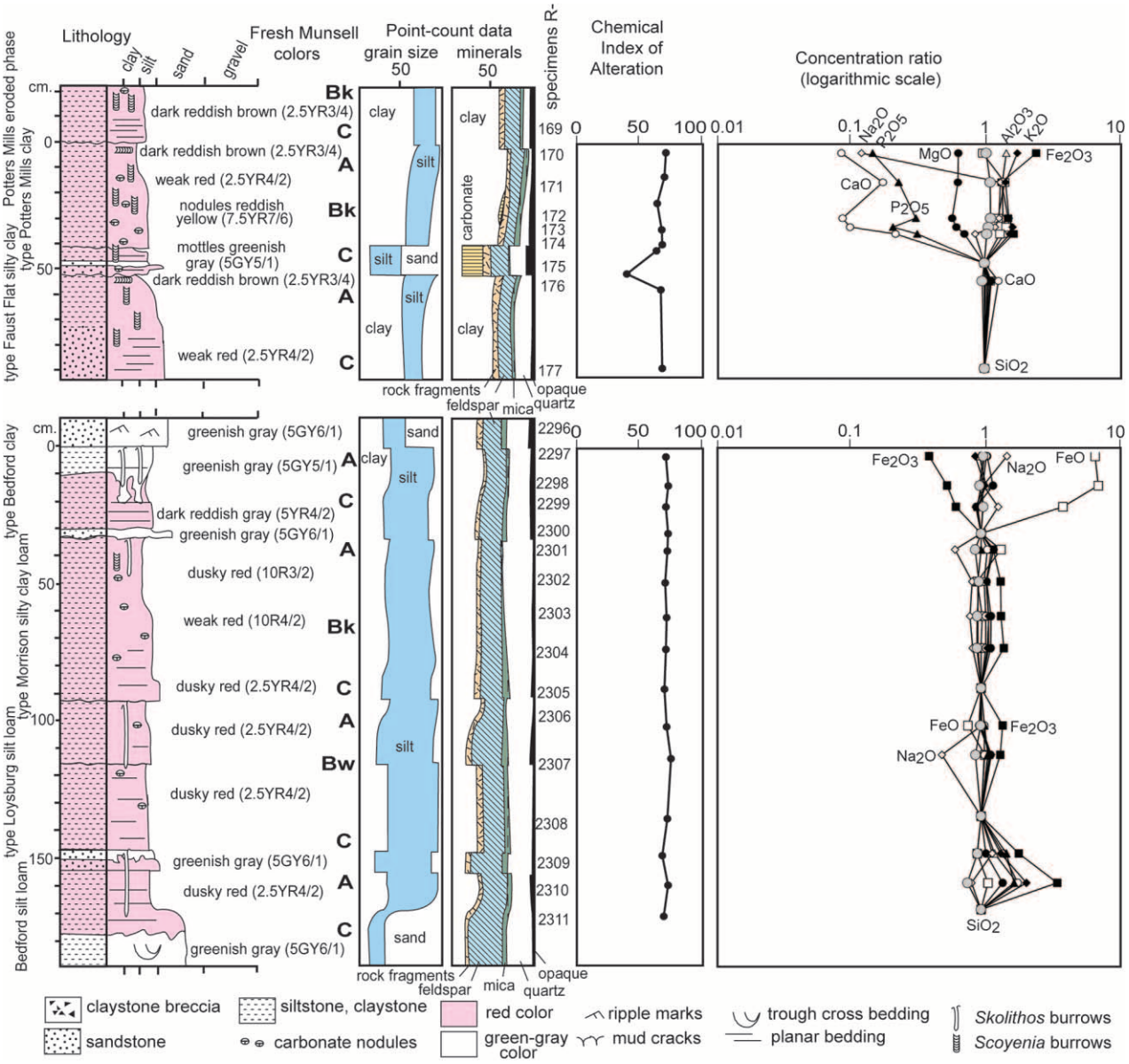


**Figure 5.** Petrographic data, chemical index of alteration values, and concentration ratios for Ordovician paleosols of the Juniata Formation (Late Silurian Beans Gap and Powell Mountain pedotypes of the Juniata are described in Driese and Foreman 1991). Colors are from a Munsell chart, sand-silt-clay and mineral proportions are from point counting, and molecular weathering ratios were calculated from major-element chemical analysis of the indicated specimens from the Condon Fossil Collection, Museum of Natural and Cultural History, University of Oregon.

***Analysis of Chemical Weathering.*** The most important weathering reaction on Earth is hydrolysis, which supplies cations to fuel plant and fungal production of acid and reduces both the volume and the mass of soil consumed (Paton et al. 1995). Hydrolysis is incongruent dissolution of weatherable minerals, such as feldspar and biotite, in carbonic acid from soil carbon dioxide to produce clay and cations in solution (van Breemen et al. 1983; Chadwick and Chorover 2001). The most common of these cations are $Ca^{2+}$, $Mg^{2+}$, $Na^{+}$, and $K^{+}$, whose abundance at different levels within a paleosol can be determined by major element chemical analysis. One common measure of overall hydrolysis is the chemical index of alteration ($I$ [mole fraction]), calculated from molar proportions (m) of alumina, lime, potash, and soda according to eq. (2) (Nesbitt and Young 1982). The lime is noncarbonate lime.

$$I = \frac{100(\mathrm{mAl_2O_3})}{\mathrm{mAl_2O_3} + \mathrm{mCaO} + \mathrm{Na_2O} + \mathrm{mK_2O}}. \qquad (2)$$

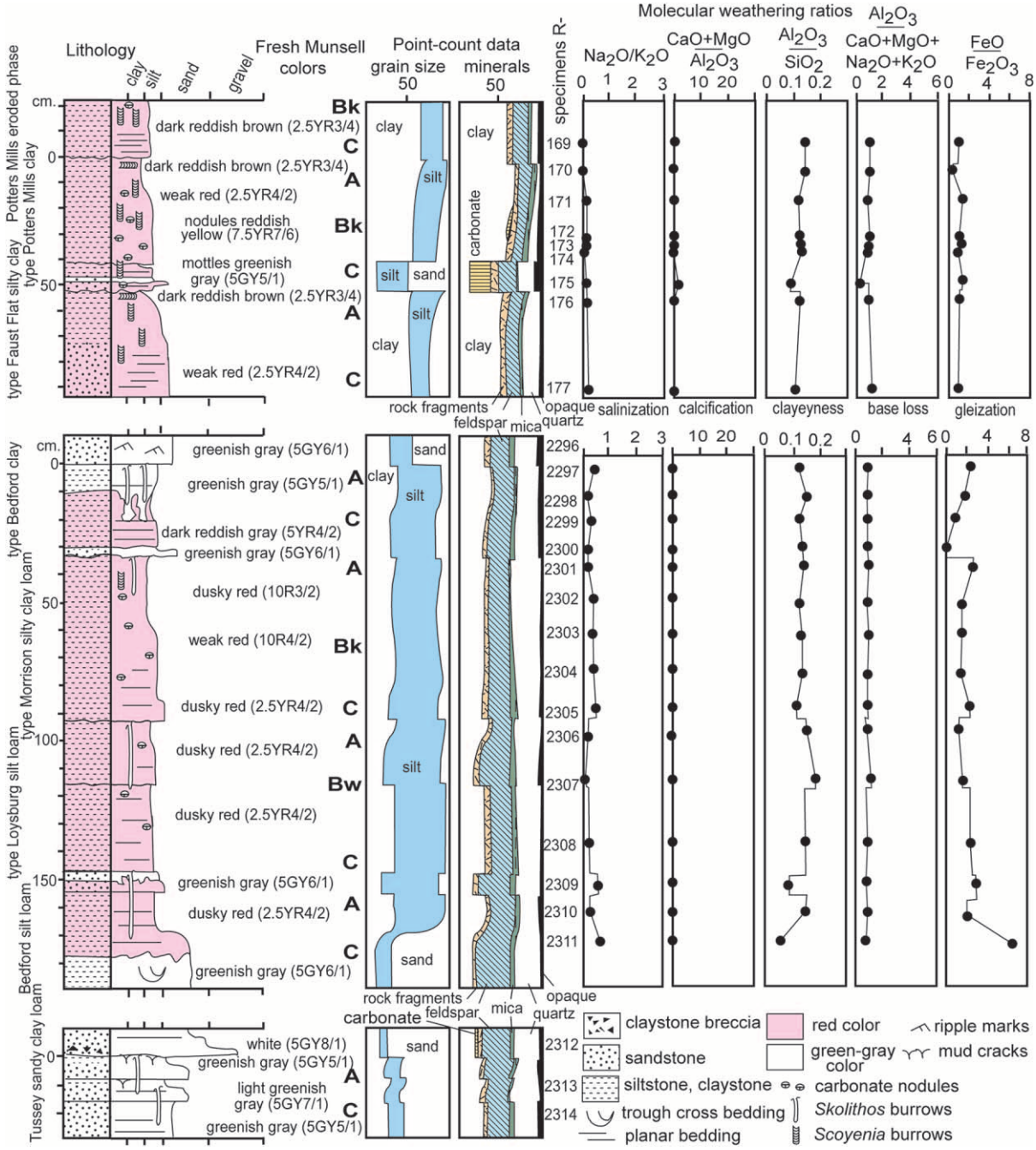


**Figure 6.** Petrographic data and molecular weathering ratios of Ordovician paleosols for the Juniata Formation (Late Silurian Beans Gap and Powell Mountain pedotypes of the Juniata are described in Driese and Foreman 1991). Colors are from a Munsell chart, sand-silt-clay and mineral proportions are from point counting, and molecular weathering ratios were calculated from major-element chemical analysis of the indicated specimens from the Condon Fossil Collection, Museum of Natural and Cultural History, University of Oregon.

The chemical index of alteration is highest near the surface of moderately developed Potters Mills and Bedford pedotypes but shows less variation within weakly developed alluvial paleosols (fig. 5). Chemical index of alteration values for Ordovician paleosols are similar to those produced by weathering in temperate climatic source terrains (Passchier and Krissek 2008).

A better indication of individual paleosols in alluvium are major oxide concentration ratios of individual beds down to likely parent material, following Grandstaff et al. (1986), which reveals the

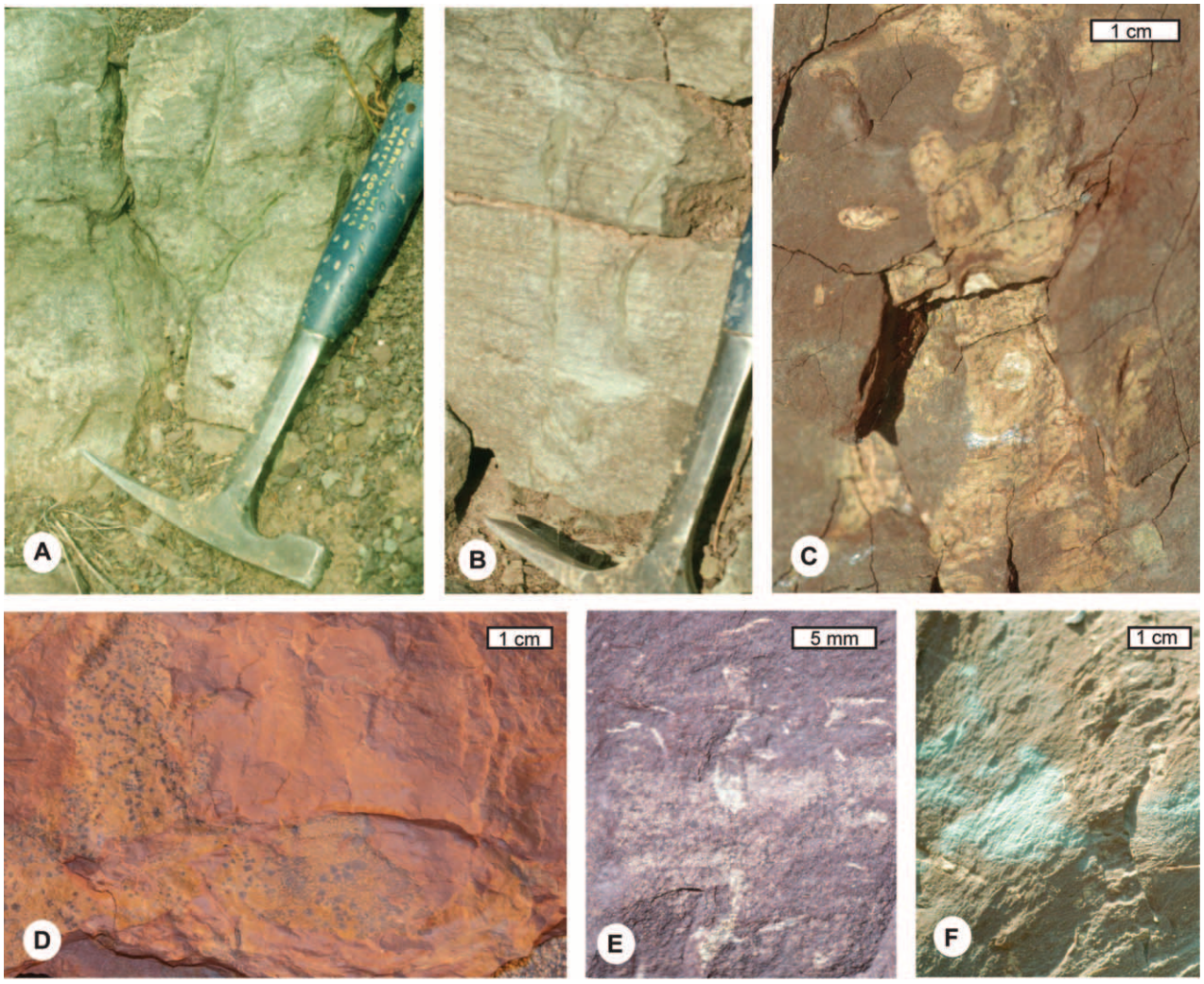


**Figure 7.** Ordovician fossil plantlike remains. *A*, *B*, *Lepidotruncus* sp. indet. from above Bedford pedotype at Beans Gap, Tennessee. *C*, *Radix* sp. indet. from Faust Flat pedotype at Potters Mills, Pennsylvania. *D*, Unidentified impression (thalloid liverwort?) dotted with black iron-manganese nodules from type Potters Mills clay paleosol at Potters Mills. *E*, Unidentified laterally branching calcite tubes (leafy liverwort?) from Faust Flat pedotype at Potters Mills. *F*, Gray-green mottle surrounded by smaller tubular mottles in red siltstone of the type Potters Mills clay from Potters Mills (*D–F*). *A–C* and *F* are field photographs, but others are in the Condon Fossil Collection, Museum of Natural and Cultural History, University of Oregon (P16295 [*D*], F35150 [*E*]).

Potters Mills clay as the most deeply weathered of the paleosols and the Faust Flat silty clay as the least weathered (fig. 5). Molecular weathering ratios of alumina over bases are also evidence for hydrolysis in the various paleosols in proportion to observed physical and petrographic degree of soil formation (fig. 6). Other molecular weathering ratios are designed to evaluate differences between paleosols in gleization (ferrous/ferric iron), salinization (soda/potash), calcification (alkaline earths/alumina), and clay formation (alumina/silica). Salinization, calcification, and gleization are subdued and clay formation marked in Potters Mills and Bedford pedotypes compared with other paleosols (fig. 6).

Weathering trends within beds are most effectively explored by tau analysis (Brimhall et al. 1992). The mass transfer of elements in a soil at a given horizon ($\tau_{w,j}$ [mole fraction]) can be calculated from the bulk density of the soil ($\rho_w$ [g cm$^{-3}$]) and parent material ($\rho_p$ [g cm$^{-3}$]) and from the chemical concentration of the element in soils ($C_{j,w}$ [weight %]) and parent material ($C_{p,w}$ [weight %]). Changes in volume of soil during weathering (strain) are estimated from an immobile element in soil (such as Ti,

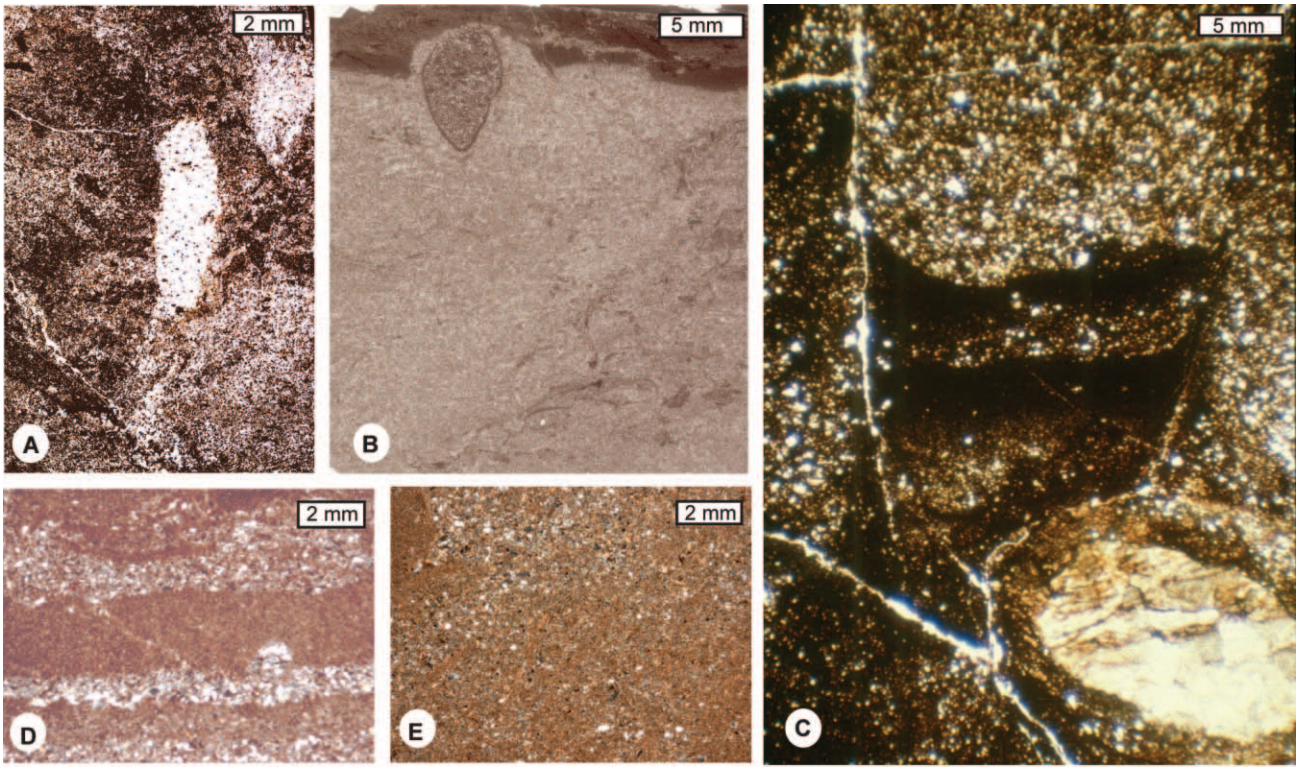


**Figure 8.** Bioturbation of Ordovician paleosols in thin section. *A*, Sand-filled *Skolithos* burrows from A horizon type Faust Flat silty clay paleosol at Potters Mills, Pennsylvania. *B*, Clay-lined surface cavity (spider or millipede egg chamber) and indistinct subsurface bioturbation from the uppermost A horizon of the type Morrison silty clay loam at Loysburg, Pennsylvania. *C*, Likely millipede burrow of *Scoyenia beerboweri* truncating pedogenic micrite and truncated by pedogenic micrite around a tubule with a sparry center. *D*, *Skolithos* burrow and relict bedding from the lower Bk horizon of the type Morrison silty clay loam at Loysburg. *E*, Indistinct bioturbation and birefringence fabric (porphyroskelic mosepic fabric) from the lower A horizon of the type Bedford clay paleosol at Loysburg. Specimen numbers are F36212 (*A*), R2301 (*B*), F36211 (*C*), R2303 (*D*), and R2298 (*E*), Condon Fossil Collection, Museum of Natural and Cultural History, University of Oregon.

used here) compared with parent material ($\varepsilon_{i,w}$ [mole fraction]). This strain is restricted to the centimeter to meter thicknesses of a single paleosol profile, whereas burial compaction acts over kilometers (Sheldon and Retallack 2001). The relevant equations (3) and (4) (below) are the basis for calculating divergence from parent material composition (origin in fig. 9). Subscripts in these equations are for immobile ($i$) and studied ($j$) element and for soil ($w$) and parent ($p$) material.

$$\tau_{j,w} = \frac{\rho_w C_{j,w}}{\rho_p C_{j,p}}(\varepsilon_{i,w} + 1) - 1, \quad (3)$$

$$\varepsilon_{i,w} = \frac{\rho_p C_{i,p}}{\rho_w C_{i,w}} - 1. \quad (4)$$

Tau analysis of selected beds in the Juniata Formation (fig. 9) does not fall into the dilate-and-gain field of both marine sediment accumulation and diagenetic processes, such as illitization and albitization (Maynard 1992). Juniata Formation beds show collapse and loss of weatherable bases and collapse and gain of sesquioxides, as in comparable Miocene alluvial calcareous paleosols (Retallack 1991). Miocene paleosols were chosen for comparison, rather than soils, because they have already been modified by burial compaction, which reduces strain and mass transfer to a more muted signal than in soils. The observed collapse occurs because depletion due to weathering has concentrated weather-resistant minerals (such as ilmenite) and elements (such as Ti) in the upper parts of beds, as in soils, rather than concentrated heavy minerals at the base of the bed, as in graded sedimentary beds (Brimhall et al. 1992). The loss of some elements occurs because the surfaces of the beds have been depleted in weatherable cations, as in soils, rather than cation enriched, as in marine clays (Feakes and Retallack 1988). Gain of alumina is due to clay formation in the surface of the

**Table 1.** Pedotypes of the Juniata and Bald Eagle Formations

| Pedotype | Diagnosis | Type example (level in m relative to Reedsville section) | Paleosol classification (Mack et al. 1993) | US taxonomy (Soil Survey Staff 2010) | FAO map (Food and Agriculture Organization 1974) | Old Australian (Stace et al. 1968) | New Australian (Isbell 1998) |
|---|---|---|---|---|---|---|---|
| Beans Gap | Red (5R) clayey (A) horizon with drab (5Y) and pyritized *Skolithos* over slickensided thick (90 cm) clayey (Bw) horizon | Beans Gap clay 723 m at Beans Gap | Vertisol | Hapludert | Chromic Vertisol | Brown Clay | Brown Vertosol |
| Bedford | Greenish gray (5GY) bedded siltstone (A) with *Skolithos* over red (5YR) bedded siltstone (C) | Bedford clay 58 m at Loysburg | Protosol | Fluvent | Eutric Fluvisol | Alluvial Soil | Stratic Rudosol |
| Faust Flat | Thin (18 cm) red (2.5YR) silty clay (A horizon) with abundant *Scoyenia* burrows over red (2.5YR) bedded sandstone (C) horizon | Faust Flat silty clay 624 m at Potters Mills | Protosol | Psamment | Earthy Sand | Earthy Sand | Lutic Rudosol |
| Loysburg | Red (2.5YR) siltstone (A) with *Scoyenia* over red (2.5YR) siltstone with shallow (12–14 cm) scattered small nodules of dolomite and calcite (Bk) | Loysburg silt loam 57 m at Loysburg | Calcisol | Calciustept | Calcic Cambisol | Desert Loam | Calcenic Tenosol |
| Morrison | Red (10R) siltstone with *Scoyenia* over shallow (18 cm) common nodules of dolomite and calcite (Bk) | Morrison silty clay loam 57.5 m at Loysburg | Calcisol | Vertic Haplocalcid | Calcic Cambisol | Desert Loam | Hypocalcic Calcarosol |
| Potters Mills | Red (2.5YR) clayey surface with drab (5Y) mottles and abundant *Scoyenia* burrows over shallow (19–36 cm) horizon (Bk) of small dolomitic and calcitic nodules | Potters Mills clay 625 m at Pottters Mills | Calcisol | Ustic Haplocalcid | Calcic Xerosol | Calcareous Red Earth | Calcic Calcarosol |
| Powell Mountain | Red (5R) slickensided clayey (A) horizon with drab (10Y) dolomitic mottles over red (10R) bioturbated claystone and drab (10Y) dolomitic and phosphatic siltstone with *Lingula* | Powell Mountain clay just below Clinch Sandstone at Powell Mountain | Protosol | Sulfaquept | Thionic Fluvisol | Wiesenboden | Supratidal Hydrosol |
| Tussey | Greenish gray (5GY) bedded siltstone (A) with *Skolithos* burrows over bedded greenish gray (5GY) sandstone | Tussey sandy clay loam 39 m at Loysburg | Protosol | Psammaquent | Eutric Gleysol | Alluvial Soil | Oxyaquic Hydrosol |

**Table 2.** Paleoenvironmental Interpretation of the Juniata and Bald Eagle Formations

| Pedotype | Paleoclimate | Vegetation | Animals | Paleotopography | Parent material | Time of formation (k.yr. ago) |
|---|---|---|---|---|---|---|
| Beans Gap | Subhumid (mean annual precipitation, 720 ± 182 mm) temperate (mean annual temperature, 11.4° ± 4.4°C), with marked dry season | Unknown | Worms (*Skolithos*) and brachiopods (*Lingula*) | Coastal plain | Smectite clay | ~10 |
| Bedford | Not diagnostic of climate | Nematophtyes (*Lepidotruncus fortis*, *Radix corrugatus*) | | Alluvial levees | Quartzo-feldspathic silt and sand | ~.1 |
| Faust Flat | Not diagnostic of climate | Nematophtyes (*Radix corrugatus*) | Millipedes (*Scoyenia beerboweri*) and worms (*Skolithos*) | Alluvial levees | Quartzo-feldspathic silt and sand | ~.1 |
| Loysburg | Subhumid (mean annual precipitation, 810 ± 182 mm) temperate (mean annual temperature, 10.9° ± 4.4°C) | Unknown | Millipedes (*Scoyenia beerboweri*) and worms (*Skolithos*) | Alluvial terraces | Quartzo-feldspathic silt | 3.9 ± 1.8 |
| Morrison | Subhumid (mean annual precipitation, 607 ± 182 mm) temperate (mean annual temperature, 9.6° ± 4.4°C) | Unknown | Millipedes (*Scoyenia beerboweri*) and worms (*Skolithos*) | Alluvial terraces | Quartzo-feldspathic silt | 5.0 ± 1.8 |
| Potters Mills | Subhumid (mean annual precipitation, 827 ± 182 mm) temperate (mean annual temperature, 11.0° ± 4.4°C) | Thalloid liverwort-like plants | Millipedes (*Scoyenia beerboweri*) | Alluvial terraces | Quartzo-feldspathic silt | 6.8 ± 1.8 |
| Powell Mountain | Not diagnostic of climate | Unknown | Worms (*Skolithos*) and brachiopods (*Lingula*) | Supratidal flat | Smectite clay and dolomite | ~.1 |
| Tussey | Not diagnostic of climate | Unknown | Worms (*Skolithos*) | Estuarine sand flats | Quartzo-feldspathic silt | ~.1 |

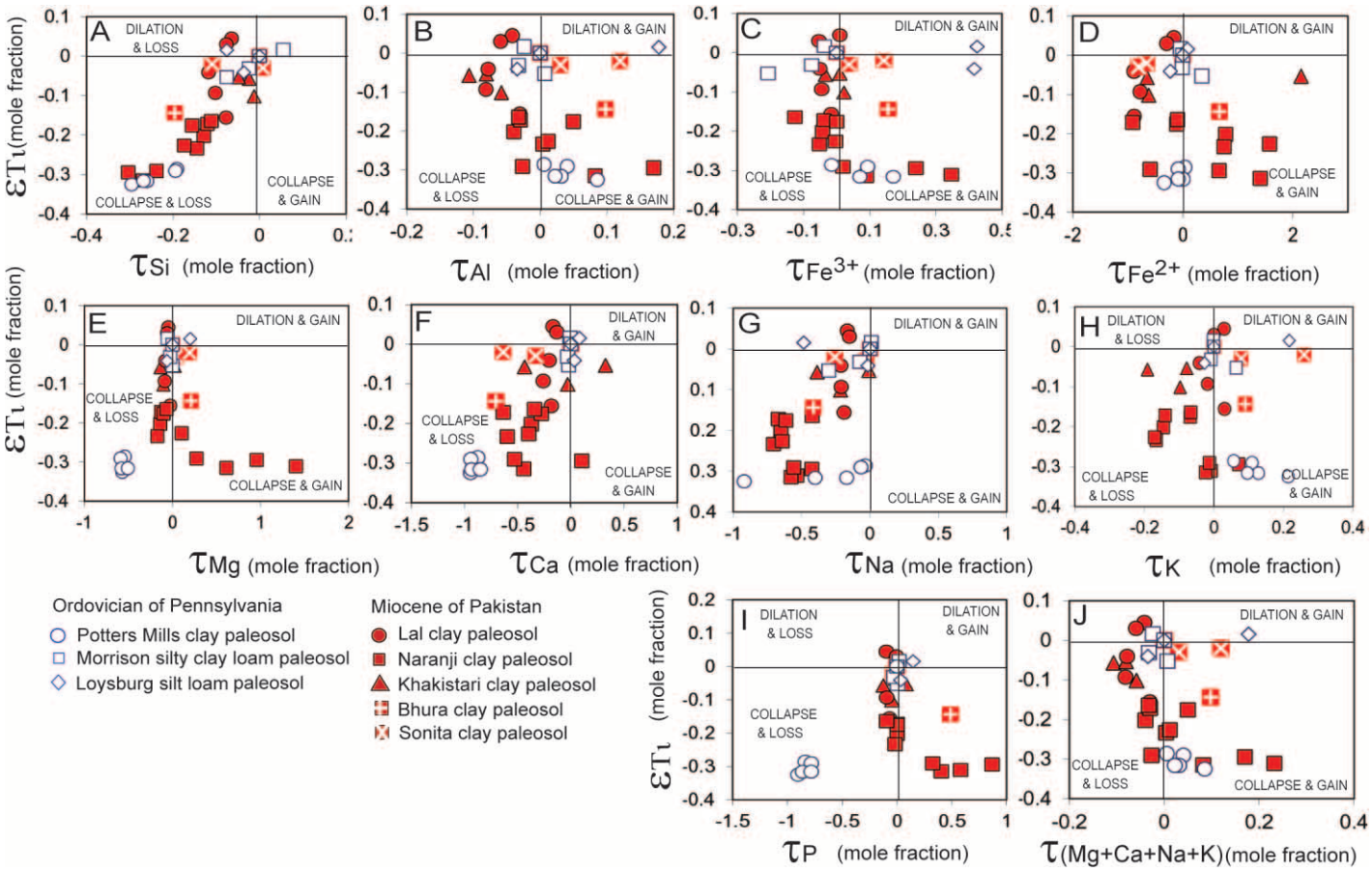


**Figure 9.** Mass transport ($\tau$) and strain ($\varepsilon$) in three kinds of Ordovician paleosols from Pennsylvania, compared with a variety of late Miocene paleosols from Pakistan, which are also in a deeply buried sequence of calcareous red paleosols (Retallack 1991).

paleosols, and gain in potash may reflect burial diagenesis (Feakes and Retallack 1988; Fedo et al. 1995). The few samples in dilate-and-gain quadrants of figure 9 reflect sedimentary additions to the tops of the paleosols (cumulic horizons; Retallack 1991, 2000). Tau analysis also reveals a different degree of weathering: Potters Mill profiles are more weathered than Morrison or Loysburg profiles, and these Ordovician paleosols overlap trends of Miocene paleosols of comparable calcareous red beds (fig. 9).

Tau analysis also reveals that these paleosols were biologically active because phosphorus depletion in soils depends on ligands released by microbes (Neaman et al. 2005). The main source mineral for phosphorus in soils is apatite, which is relatively inert to carbonic acid attack. Weathering of phosphorus and alkali and alkaline earth bases in Ordovician soils is direct evidence for biotic enhancement of weathering inferred by carbon cycle models (Berner 2006).

***Isotopic Fractionation of Pedogenic Carbonate.*** A distinctive isotopic signature diagnostic of carbonate in paleosols (fig. 10*A*) and soils (fig. 10*B*) is correlation of $\delta^{13}C$ and $\delta^{18}O$ values (Knauth et al. 2003; Huang et al. 2005; Ufnar et al. 2008; Retallack et al. 2014). Such tight correlations are inherited from the same covariance seen in respired soil $CO_2$ (Ehleringer and Cook 1998; Ehleringer et al. 2000), and that in turn is derived from the same covariance observed in plant cellulose (Barbour et al. 2002). These observations confirm models that show that carbon and oxygen isotopic covariance is due to selection of light isotopologs of $CO_2$ during its diffusion into cells and consumption by photosynthesis (Barbour and Farquhar 2000). Carbon-oxygen isotopic covariance is a characteristic ecosystem relationship (Barbour et al. 2002), with strongest correlations in semiarid communities of mixed $C_3$-$C_4$ photosynthetic pathways and seasonal variations in moisture and plant productivity (Liu et al. 2014). The slope of the relationship shows a positive relationship with mean annual vapor pressure deficit (kPa), or the difference between moisture in air and the amount a plant can hold when saturated, a measure of evapotranspiration (Barbour et al. 2002).

Marine limestone altered by surface weathering also shows positive correlation (fig. 10*D*). Such alteration is commonly called burial diagenesis but is due to dissolution and replacement from percolation of meteoric water, sometimes to exceptionally deep levels well below current sea level during the last glacial maximum (Lohman 1988; Melim et al. 2004). Lacustrine marls may also show modest positive correlations ($r^2$ of 0.4–0.6), attributed to closed basin hydrology (Talbot 1990) or climate change (Drummond et al. 1995) but perhaps also due to meteoric alteration (Melim et al. 2004) or cellulose respiration (Ehleringer et al. 2000). These correlations and low values are easily distinguished from unaltered marine limestone (fig. 10*E*), which clusters near 0 for both $\delta^{13}C$ and $\delta^{18}O$ of modern sea shells (Veizer et al. 1999) and is more negative than modern for $\delta^{18}O$ in Ordovician (Prokoph et al. 2008) and Cambrian (Surge et al. 1997) marine limestones. The long-term secular increase in $\delta^{18}O$ values for sea water may be related to changes in ocean crust hydrothermal regime (Kasting et al. 2006). For these reasons, marine limestones with indistinct correlations between $\delta^{13}C$ and $\delta^{18}O$ are poor indicators of paleoclimate, mixing signals of original sea water and later weathering (Lohman 1988; Melim et al. 2004). In contrast, pedogenic carbonate with tight correlations preserve original soil signals (Knauth et al. 2003; Huang et al. 2005; Ufnar et al. 2008; Retallack et al. 2014).

Also distinctive is a pattern of near constant $\delta^{18}O$ but highly varied $\delta^{13}C$ in carbonate of marine methane cold seeps (fig. 10*F*; Aiello et al. 2001). Methanogenic carbonate $\delta^{13}C$ is extremely negative: down to –48‰ in marine methane seeps (Peckmann et al. 2002) and to –43‰ in wetland paleosols (Ludvigson et al. 2013). This "meteoric oxygen line" pattern arises because of the dominance of $\delta^{18}O$ composition by water in waterlogged to aquatic habitats.

Tight correlations of $\delta^{13}C$ and $\delta^{18}O$ are observed only for soils of similar vegetation and climate (fig. 10*B*) and paleosols of particular geological formations (fig. 10*A*) because the isotopic composition of soil $CO_2$ varies with vegetation and climate (Ufnar et al. 2008). Moderately significant correlations and surprisingly positive values for both $\delta^{13}C$ and $\delta^{18}O$ are found on modern carbonate crusts on basalt (fig. 10*C*).

***Fossil Plants.*** The Juniata Formation predates the oldest known vascular land plant megafossils: Silurian (Ludlovian) *Baragwanathia longifolia* with *Bohemograptus bohemicus* graptolites (426 Ma) from Victoria, Australia (Rickards 2000), and *Cooksonia pertoni* in the *Saetograptus leintwardiensis* graptolite zone (425 Ma) in Wales (Cleal and Thomas 1995). Molecular-clock ages of Ordovician have been determined for liverworts (475 Ma) and mosses (458 Ma), but ages of Silurian have been determined for hornworts (440 Ma) and vascular land plants (422 Ma; Magallón et al. 2013). Ordovician plants have been considered bryophytes, but recent research on early land plants suggests several extinct prebryophytic lineages, and a better term for nonvascular Ordovician-Silurian plants is "cryptophytes" (Edwards et al. 2014). There is also evidence from palynology for glomalean fungi (Redecker et al. 2000) and cryptophytes (Steemans et al. 2010; Kenrick

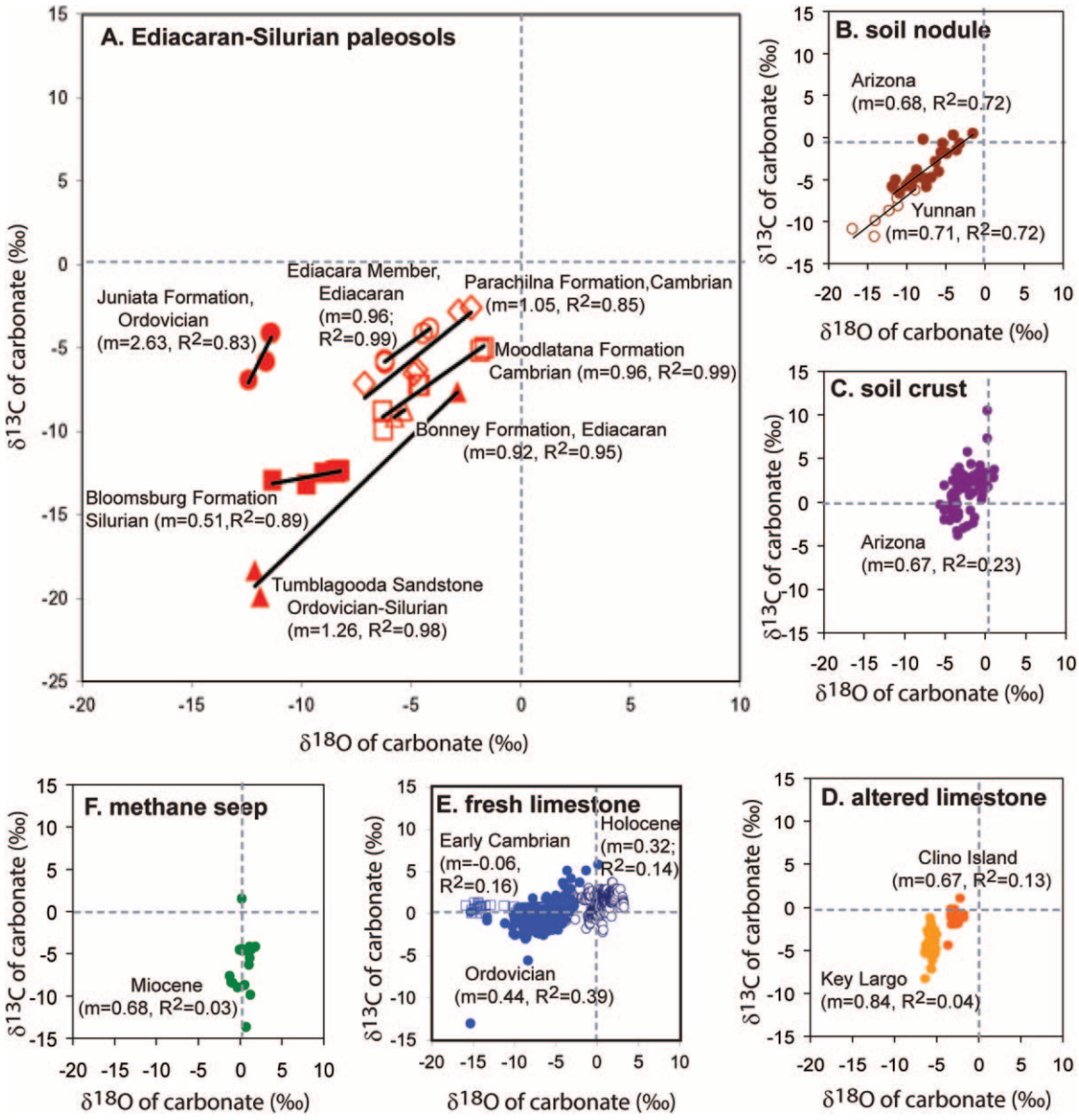


**Figure 10.** Carbon and oxygen isotopic composition of carbonate in (*A*) Ordovician paleosols of Pennsylvania (Retallack 1993) and Australia (Retallack 2009*b*), compared with Ediacaran and Cambrian paleosols of Australia (Retallack et al. 2014) and Silurian paleosols of Pennsylvania (Harrisburg data of King 1998); (*B*) soil nodules (above Woodhouse lava flow, near Flagstaff, AZ, from Knauth et al. 2003; and in Yuanmou Basin, Yunnan, China, from Huang et al. 2005); (*C*) soil crusts on basalt (Sentinel Volcanic Field, AZ, from Knauth et al. 2003); (*D*) Quaternary marine limestone altered diagenetically by meteoric water (Key Largo, FL, from Lohman 1988 and Clino Island, Bahamas, from Melim et al. 2004); (*E*) Holocene (open circles) and Ordovician (open squares) unweathered marine limestones (Veizer et al. 1999; Prokoph et al. 2008) and early Cambrian (filled circles), Ajax Limestone, South Australia (Surge et al. 1997); and (*F*) marine methane cold seep carbonate (Miocene, Santa Cruz Formation, Santa Cruz, CA, from Aiello et al. 2001). Slope of linear regression (*m*) and coefficients of determination ($R^2$) show that carbon and oxygen isotopic composition is significantly correlated in soils and paleosols.

et al. 2012) during the Katian and Hirnantian. This kind of low, clumped vegetation of well-drained soils has been called a polsterland by Retallack (1992), comparable with modern bryophytic soil crusts of deserts (Belnap et al. 2003). Carbonaceous remains from Ordovician and Silurian rocks of Appalachia have the distinctive carbon isotopic composition of land plants (Tomescu and Rothwell 2006; Tomescu et al. 2009) but represent wetland marsh and microbial mat communities distinct from the

dryland vegetation represented by most of the red calcareous paleosols described here (Feakes and Retallack 1988).

Fossil impressions and drab mottles in the Juniata Formation are suggestive of thallose liverworts (fig. 7*D*), but some are comparable with leafy liverworts (fig. 7*E*). Also locally common, particularly in Tussey and Faust Flat pedotypes, are stout casts of irregularly wrinkled trunks engulfed in crossbedded sandstone, with branching and anastomosing, rugulose, rootlike structures (fig. 7*A*, 7*B*). Some of these strata-transgressive structures are preferentially encrusted with pedogenic carbonate (fig. 7*C*). These various trunks are comparable with fossil trunks described as *Lepidotruncus fortis* (Fritsch 1908) and rootlike structures, *Radix corrugatus* (Fritsch 1908), from the Katian-Hirnantian (Kříž and Pojeta 1974), Kosov Formation, near Chodouň and Vonoklas (respectively), Czech Republic. Comparable remains (here referred to as *Lepidotruncus* sp. indet.) are known from Hirnantian glacial deposits of the El Golea Member, Tamadjert Formation, near Zmeïlet Barka, Algeria (Arbey and Koeniguer 1979; Le Heron and Craig 2008). More informative comparable remains (here referred to *Radix* sp. indet.) are known from the early Katian Gull River Formation near Ingham Mills, New York (Argast 1992). The New York *Radix* is partly permineralized in calcite and shows a distinctive histology of tubular cell walls with a carbon isotopic composition ($\delta^{13}C_{organic}$ vs. Pee Dee belemnite [PDB] of −23.5‰ to −25‰) of land plants rather than marine organic matter (Tomescu et al. 2009). The tubular histology is comparable with that of Devonian *Prototaxites logani*, the best preserved of nematophytes, interpreted as a giant basidomycete fungus by Hueber (2001; Boyce et al. 2007), a lichen by Retallack and Landing (2014), and a rolled mat of liverworts by Graham et al. (2010). Rolled mat is not plausible for these Ordovician rootlike and current resistant structures because they are strata-transgressive (fig. 7*A*–7*C*). Other terrestrial nematophytes are known from Early Ordovician sandstones (Grindstone Range Sandstone near Wirrealpa, South Australia; Retallack 2009*a*) and Middle Cambrian phosphorites (Beetle Creek Formation at Mount Murray, Queensland; Fleming and Rigby 1972; Southgate 1986).

***Trace Fossils.*** The diversity of trace fossils in beds of a particular pedofabric in the Juniata Formation is low, usually only *Skolithus* and *Scoyenia* (table 2). The other ichnogenera of trace fossils known from the Juniata Formation (cf. *Diplichnites*, *Circulichnus*, *Helminthopsis*?, *Palaeophycus*, *Planolites*, *Scolicia*?; Retallack 1985, 2000; Diecchio and Hall 1998; Davies et al. 2010; Retallack et al. 2011) are in lacustrine interbeds or weakly developed paleosols. Comparable low-diversity trace fossil assemblages are found elsewhere in Cambrian-Ordovician fluvial and lacustrine rocks (Trewin and McNamara 1994; Mikuláš 1995; Retallack 2008, 2009*a*, 2009*b*). The Juniata Formation has not yet yielded marine trace fossils such as *Rusophycus* or *Chondrites*, common among at least 22 ichnogenera in Ordovician (Katian) rocks with undoubted marine fossils around Cincinnati, Ohio (Osgood 1970).

Ordovician paleosols of the Juniata Formation have common burrows of invertebrates with prominent clay-silt backfills (*Scoyenia beerboweri* Retallack 2001*a*). These burrows formed during soil formation because they both cut across and are cut by micritic carbonate with microtexture (calciasepic) and isotopic composition of pedogenic carbonate (fig. 8*C*). The morphology of backfills, fecal pellets, and burrow-size distribution are compatible with the creation of *S. beerboweri* by polyzoniid or similar millipedes (Retallack 2001*b*; Retallack et al. 2011). This interpretation was challenged by Davies et al. (2010), who considered the oldest millipedes Silurian and were unaware of Late Ordovician (Sandbian) millipede trackways (Johnson et al. 1994), Cambrian millipede-like fossils (Hou and Bergström 1998; Budd et al. 2001; Retallack et al. 2011), or phylogenomic (Rota-Stabelli et al. 2013; Misof et al. 2014) and biogeographic (Shelley and Golovatch 2011) evidence for a Cambrian origin of millipedes. Another remarkable trace fossil found in thin section of the surface of the type Morrison clay paleosol (fig. 8*B*, upper left) is a clay-lined structure, within an excavated hollow, containing organic lined spherical structures. This enigmatic fossil is comparable with egg and molt chambers of millipedes (Romell 1935; Toye 1967).

Other common trace fossils in the Juniata Formation include remains comparable with *Skolithos* (fig. 8*A*), *Circulichnus*, *Scolicia*, *Planolites*, *Palaeophycus*, and *Helminthopsis* (Diecchio and Hall 1998; Davies et al. 2010), all commonly attributed to wormlike or sluglike organisms.

Also found in the Juniata Formation are rare trackways up to 3 cm wide of arthropods (Diecchio and Hall 1998; Davies et al. 2010), comparable with older Ordovician *Diplichnites gouldii* from the Middle Ordovician (Dapingian) part of the Tumblagooda Sandstone of Kalbarri, Western Australia (Trewin and McNamara 1994; Retallack 2009*b*), and Early Ordovician (Tremadocian) lower Grindstone Range Sandstone of Wirrealpa, South Australia (Retallack 2009*a*). These Australian Ordovician trackways were attributed to large amphibious euthycarcinoids, such as *Kalbarria brimmellae* (McNamara and Trewin 1993).

Marginal marine trace fossils (*Skolithos verticalis*) penetrate a firmground atop the Beans Gap clay paleosol near the top of the Juniata Formation at Beans Gap, Tennessee (fig. 4*A*). In this case, transitional marine origin is betrayed by local gleization with pyritization and phosphatization as well as lingulid brachiopod fragments (Driese and Foreman 1991). Ordovician marine bioturbation was thorough and deep (Sheehan and Schiefelbein 1984), but coeval physical disruption of soils was far from negligible.

## New Interpretations of Paleosols

Red, clayey, fractured, and nodularized beds of the Juniata Formation do indeed appear to be paleosols (Retallack and Feakes 1987; Feakes and Retallack 1988; Retallack 1993; Driese and Foreman 1991, 1992), and they have much to tell us about Ordovician terrestrial environments and life on land (fig. 11).

***Parent Material.*** The Juniata and Bald Eagle Formations are quartzofeldspathic in mineral composition, derived from erosion of preexisting sedimentary rocks, such as the Martinsburg Formation in the Taconic Mountains to the east (Thompson 1999). There is a surprising amount of feldspar in the sandstones and claystones (figs. 5, 6) compared with Mesozoic and Cenozoic sediments (Retallack 1991, 1997). These differences in other early Paleozoic sandstones have been attributed to a different regime of weathering before the advent of vascular land plants (Dott 2003; Jutras et al. 2009). Tau analysis of paleosols does indicate less mobilization of potash from Ordovician than Miocene paleosols (fig. 9). Parent material composition of the soils that supplied sediment to the Juniata Formation is known only in general terms, but this article considers mainly soil formation forward from single beds of weathered alluvium as a parent material (figs. 5, 9).

***Paleotopography.*** The Juniata and Bald Eagle Formations have long been interpreted as deposits of sheet-braided streams draining a coastal plain to the west of the Taconic Mountains (Cotter 1978). Abundant burrows (*Scoyenia beerboweri*) in many of the paleosols are evidence that those soils were well drained and presumably elevated on alluvial terraces above paleochannels (Retallack 2001*a*). *Scoyenia*-bearing paleosols of the Juniata Formation are red and highly oxidized, but the Bald Eagle Formation and the uppermost Juniata Formation also have paleosols that are entirely or partially gray-green due to early burial gleization (Thompson 1970*a*). The drab paleosols also have a different assemblage of trace and body fossils, including *Skolithos* and *Lepidotruncus*. These paleontological differences can be related to slow drainage of gray-green paleosols, closer to alluvial water table or inundated by coastal lagoons with lingulid and rhynchonellid brachiopods (Schuchert 1916; Dreise and Foreman 1992).

***Time for Formation.*** A useful proxy for the time over which a paleosol formed is the size of carbonate nodules in paleosols (Retallack 2005). In modern soils, the diameter of nodules ($S$) is related to soil age ($A$ [ka]) by equation (5) ($R^2 = 0.57$; SE, 1.8 ka; Retallack 2005).

$$A = 3.92S^{0.34}. \quad (5)$$

Burial compaction has a minor flattening effect on carbonate nodules but cannot alter their horizontal diameter because of lithostatic pressure from the side (Sheldon and Retallack 2001). This proxy is unlikely to be compromised by lack of vascular land plants because the formation of soil carbonate is considered largely microbial (Monger et al. 1991).

The results of these calculations show soil durations of 4–7 k.yr. for carbonate in Ordovician paleosols. For the 116-m measured section at Potters Mills (21% of the whole section of Juniata Formation at Reedsville), the durations for 8 Potters Mills and 11 Faust Flat paleosols add up to a total duration of 55,500 yr. For the 34-m measured section at Beans Gap (6% of the whole section of Juniata Formation at Reedsville), the durations add up to a total duration of 54,100 yr. If these sections represent the interval of low Hirnantian sea level, dated at 445.2–443.8 Ma (Gradstein et al. 2012), this 1.4 m.yr. is 25 times the duration represented by paleosols. Such discrepancies are normal for geological versus paleosol estimates of geological time of Cenozoic paleosol sequences, which are rife with both major and minor disconformities (Retallack 1998).

***Paleoproductivity.*** Soil productivity can be measured in a variety of ways, including secondary productivity of microbial and root-respired $CO_2$ within the soil responsible for hydrolytic supply of nutrients to plants (van Breemen et al. 1983; Chadwick and Chorover 2001). A late-growing-season soil $CO_2$ paleobarometer of Retallack (2009*c*) from modern soils instrumented for $CO_2$ content has been updated by Breecker and Retallack (2014) and relates productivity ($P_r$ [ppmv $CO_2$]) with depth to carbonate ($D_s$ [cm]) as equation (6) ($R^2 = 0.66$; SE, 766 ppmv).

$$P_r = 35.3D_s + 588. \quad (6)$$

The alternative equation for $P_r$ of Cotton and Sheldon (2012) derived from paleoprecipitation estimates of paleosols is not suitable for Devonian or older paleosols because even Devonian forests were less productive at similar isohyets than modern eco-

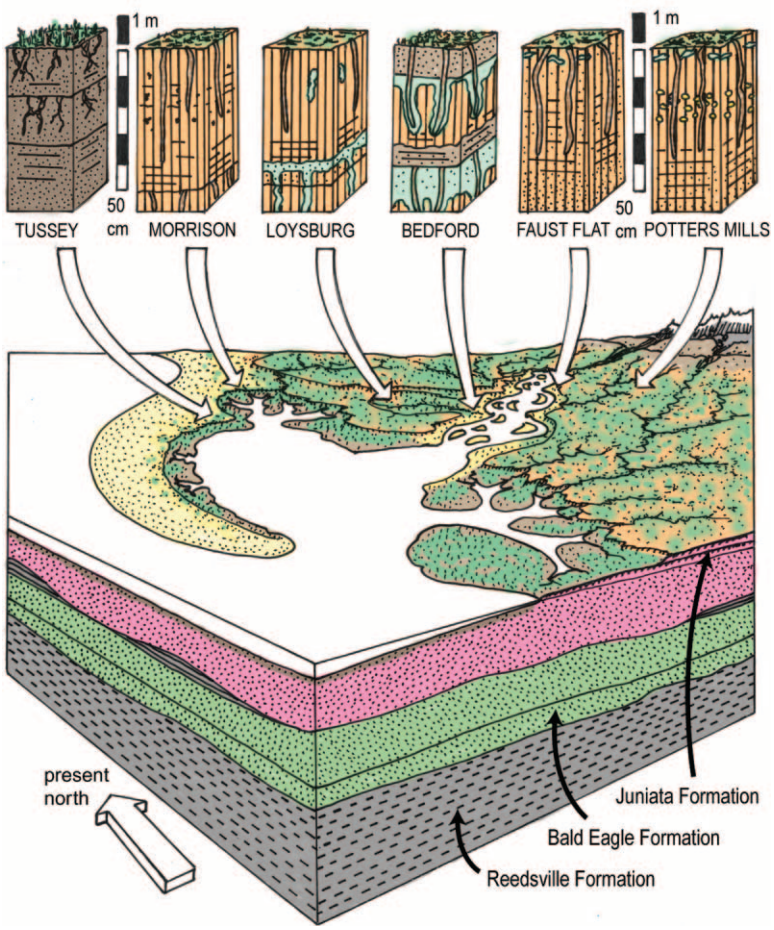


**Figure 11.** Reconstructed Ordovician soils and landscapes of the Juniata and Bald Eagle Formations in Pennsylvania. An earlier reconstruction by Feakes and Retallack (1988) showed only inland pedotypes. Beans Gap and Powell Mountain paleosols of the Juniata Formation in Tennessee (Driese and Foreman 1992) are not included because they are in a different region and are also likely to be early Silurian (fig. 3).

systems (Retallack and Huang 2011), and this article aims to quantify even lower productivity of Ordovician ecosystems. Using equation (6), respired soil $CO_2$ can be calculated for paleosols from depth to carbonate nodules once they have been corrected to original soil depths using equation (1). This proxy included desert soils in which pedogenic carbonate is mainly a microbial precipitate (Monger et al. 1991), so it is applicable to pre-Devonian paleosols.

The results of these calculations for the Late Ordovician Potters Mills clay paleosol is soil $CO_2$ of 1538 ± 766 ppmv, which is low compared with 19 other Ordovician paleosols of Pennsylvania and Tennessee showing increased depth to Bk and thus increased late-growing-season soil $CO_2$ until a Hirnantian decline (fig. 3*B*). A spike in soil secondary productivity is apparent near the Katian-Hirnantian boundary in Pennsylvania and Tennessee. This spike is not just noise in the data because it is also found in three separate sections separated by 2000 km in Western and South Australia (Retallack 2009*b*). Furthermore, it correlates with global marine isotopic Boda event and Hirnantian mass extinction (Armstrong et al. 2009*a*). Comparable paleoproductivity similar to modern desert soils, including productivity spikes, have also been calculated for 383 successive Cambrian-Silurian paleosols of the Tumblagooda Sandstone of Western Australia (fig. 12*A*; Retallack 2009*b*). Rising late Katian terrestrial productivity was coeval with rising $\delta^{13}C$ in marine carbonate (fig. 12*B*, 12*C*), which reflects increased marine productivity (Prokoph et al. 2008).

Soil $CO_2$ levels in Ordovician and Silurian aridland paleosols are significantly less than soil $CO_2$ of 26,656 ppmv determined by Yapp and Poths (1993, 1994) for a Late Ordovician paleosol capping the Neda Iron Formation in Wisconsin. This thick (1.5 m) lateritic paleosol (Retallack 2003) is very different

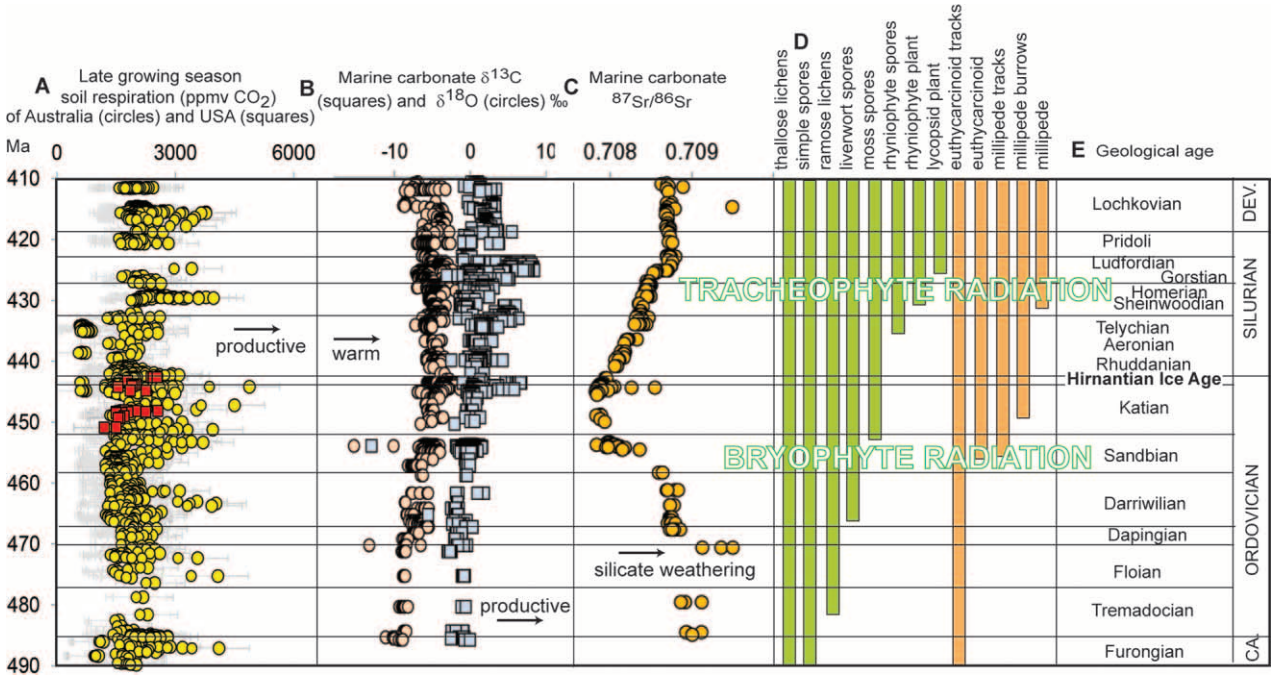


**Figure 12.** Proxies for terrestrial productivity (*A*), marine carbon cycle and paleotemperature (*B*), terrestrial weathering (*C*), and first appearance of land plants and animals (*D*). Terrestrial productivities were calculated by the method of Breecker and Retallack (2014) using Australian data of Retallack (2009*b*; circles) and North American data (herein; squares). Isotopic data are from Veizer et al. (1999) and Prokoph et al. (2008), recalibrated to the time scale of Gradstein et al. (2012). Range data are from Retallack (2008, 2009*a*, 2009*b*), Steemans et al. (2010), Retallack et al. (2011), and Kenrick et al. (2012).

from the calcareous paleosols described here and formed farther north within the tropics of the time, during the latest Katian (McLaughlin et al. 2013). Modern calcareous soils have $CO_2$ concentrations less than 12,400 ppm (Retallack 2009*c*), but modern lateritic soils have $CO_2$ concentrations up to 104,000 ppm (Matsumoto et al. 1997). The Ordovician tropical lateritic paleosol of the Neda Iron Formation thus had productivity that was only about 26% of modern lateritic soils.

The lower productivity of Ordovician compared with modern terrestrial ecosystems is more than a simple pH effect on potassium mobilization inferred by Jutras et al. (2009). Both calcareous (alkaline) and lateritic (mildly acidic) Ordovician paleosols discussed here show evidence of lower than modern productivity. Nor was the Ordovician a unique time of unusually alkaline soils between an acidifying primeval $CO_2$ greenhouse and acidifying vascular land plants (Jutras et al. 2009) because potash-rich calcareous paleosols are known in the Cambrian (Retallack 2008), Proterozoic (Driese et al. 1995), and Archean (Watanabe et al. 2004).

***Paleoprecipitation.*** Paleoprecipitation can be estimated from paleosols using the paleohyetometer of Sheldon et al. (2002) on the basis of the chemical index of alteration without potash, or CIA-K ($A = 100 \times mAl_2O_3/(mAl_2O_3 + mCaO + mNa_2O)$ [moles]), which increases with mean annual precipitation ($R$ [mm]) in modern soils ($R^2 = 0.72$; SE, 182 mm), as follows:

$$R = 221e^{0.0197A}. \quad (7)$$

This formulation is based on the hydrolysis equation of weathering, which enriches alumina at the expense of lime, magnesia, potash, and soda. Magnesia is ignored because it is not significant for most sedimentary rocks, and potash is left out because it can be enriched during deep burial alteration of sediments (Maynard 1992). This proxy is not suitable for samples with free carbonate but can be applied to carbonate-free soil above carbonate at depths comparable with Ordovician paleosols (17–47 cm before burial compaction estimated from eq. [1]). This proxy also is applicable to pre-Devonian soils with clay skins and ped structures comparable with Bw horizons (figs. 5, 6) because carbonic acid from microbial soil respiration is the principal agent of

hydrolysis (Paton et al. 1995). Unlike the bed-scale tau analysis employed here (eq. [2]), this method conflates weathering that contributed to the parent material as well as within the paleosol. An alternative paleohyetometer uses depth to carbonate nodules in soils, which increases with mean annual precipitation (Retallack 2005) but shows a closer relation to late-growing-season soil $CO_2$ (Breecker and Retallack 2014). The carbonate paleohyetometer is not suitable for Devonian or older paleosols because even Devonian forests were less productive at similar isohyets than modern ecosystems (Retallack and Huang 2011).

Estimates of paleoprecipitation based on CIA-K give subhumid mean annual precipitation: 607 ± 182 mm for Loysburg silt loam and 810 ± 182 mm for Morrison silty clay loam (both late Katian), 827 ± 182 mm for Potters Mills clay (Hirnantian), and 720 ± 182 mm for Beans Gap clay (early Llandoverian). These new estimates are preferable to earlier semiarid estimates (Feakes and Retallack 1988) because the Juniata Formation formed a coastal plain within 100 km of the sea (fig. 1*C*) and high marine productivity fueled by mineral nutrients is inferred for high marine carbonate $\delta^{13}C$ values (Hirnantian Isotope Carbon Excursion [HICE] of Young et al. 2010; Ghienne et al. 2014) and black shales (Armstrong et al. 2009*a*).

At the 827-mm isohyet in Australia today, trees are 23 ± 2.3 m tall, Bk horizons are 81 ± 5 cm deep (Retallack 2012), and late-growing-season productivity is 3448 ± 766 ppm $CO_2$ (eq. [6]). Ordovician nematophytes of the Juniata Formation are only 5% of this height, following the maximum likely scaling presented by Retallack and Landing (2014). Ordovician Bk depth was only 33% of modern and secondary productivity was only 44% of modern for this isohyet: evolutionary advances since the Ordovician have greatly increased terrestrial productivity and their effects on weathering (Berner 1997, 2006).

***Paleoclimatic Seasonality.*** Driese and Foreman (1992) described extensive slickensides in the Beans Gap and Powell Mountain clay paleosols and compared them with the structure of Vertisols, which are swelling clay soils with a marked dry season (Soil Survey Staff 2010). No mukkara structure or gilgai microrelief of Vertisols (Paton 1974) was noted in these paleosols, which are exceptional for the Juniata Formation and formed at a stratigraphic level of Silurian marine transgression (fig. 3).

Seasonality of precipitation in soils, defined as the difference in mean monthly precipitation of the driest versus the wettest month ($M$ [mm]), has been shown by Retallack (2005) to be related to the thickness of soil with carbonate or to the distance between the lowest and the highest nodule in the profile ($H_o$ [cm]), by equation (8) ($R^2 = 0.58$; SE, 22 mm).

$$M = 0.79H_o + 13.71. \quad (8)$$

For application to paleosols, the thicknesses of paleosol with carbonate must be corrected for compaction by overburden (eq. [1]). Because soil carbonate is primarily a microbial precipitate (Monger et al. 1991), this proxy can be applied to pre-Devonian paleosols with other evidence of life. Estimates of the mean annual range of precipitation are 46 ± 22 mm for the Loysburg silt loam and 42 ± 22 mm for the Morrison silty clay loam (both late Katian) and are 45 ± 22 mm for the Potters Mills clay (Hirnantian). This is moderately seasonal but not monsoonal because it is less than a third of the mean annual range of precipitation of 141–2510 mm for modern monsoonal soils (Retallack 1991, 2005). Like the monsoonal soils and paleosols, the Ordovician ones have alternately precipitated carbonate and hematite (fig. 8*C*), an indication of alternating dissolution-evaporation and reduction-oxidation (Retallack 1991). Furthermore, monsoonal carbonate nodules are often unusually abundant and small (2–4 mm) rather than scattered and large (2–5 cm; Retallack 2005).

***Paleotemperature.*** A useful paleotemperature proxy for paleosols of Óskarsson et al. (2009) is based on modern soils under tundra vegetation of Iceland. This linear regression between mean annual temperature ($T$ [°C]) and the chemical index of weathering ($I = 100 \times mAl_2O_3/(mAl_2O_3 + mCaO + mNa_2O)$ in molar proportions is given in equation (9) ($R^2 = 0.81$; SE, 0.4°C). This proxy is useful for pre-Devonian paleosols with evidence of life because of hydrolytic weathering reactions driven by soil respiration (Paton et al. 1995). Furthermore, it is based on vegetation with large proportions of nonvascular land plants, unlike other paleothermometers based on forested soils (Sheldon et al. 2002; Gallagher and Sheldon 2013).

$$T = -18.5N + 17.3. \quad (9)$$

These calculations give temperate paleotemperatures of 9.6° ± 0.4°C for the Loysburg silt loam and 9.0° ± 0.4°C for the Morrison silty clay loam (both late Katian), 10.9° ± 0.4°C for the Potters Mills clay (Hirnantian), and 10.3° ± 0.4°C for the Beans Gap clay (early Llandoverian). These estimates are cool but compatible with equally surprising evidence of Cambrian shoreline ice in Wisconsin (Runkel et al. 2010), Cambrian tillites in New Brunswick and Ireland (Landing and MacGabhann 2010), and Late Or-

dovician tillites and periglacial features of Saharan Africa (Le Heron and Craig 2008; Finnegan et al. 2011).

These paleotemperatures are also cool for paleolatitudes determined by the Point Tracker program of Scotese (1997): 27°S for the Ordovician site in Tennessee and 25°–26°S for sites in Pennsylvania. These are latitudes like those of modern Sandgate, near Brisbane, Australia, which has a mean annual temperature of 19.7°C (for 1913–1976) and a mean sea surface temperature of 23°C (for 1961–1990; Australian Bureau of Meteorology 2015). Marine temperatures estimated from $\delta^{18}O$ of conodonts in Minnesota and Kentucky are thought to have been 22°C (Buggisch et al. 2010), and those from $\Delta_{47}$ of corals from Anticosti Island, which was closer to the paleoequator, were 28°C (Finnegan et al. 2011). Late Ordovician marine limestones of the Nashville and Cincinnati domes are bryozoan-dominated (rather than coral-dominated) temperate-type carbonates (Holland and Patzkowsky 1998). Modeling based on oxygen isotopic composition of marine carbonates (Armstrong et al. 2009*b*) shows that tropical waters extended south only as far as latitude 22°S and that the intertropical convergence zone extended south as far as 10°S for only a brief interval of the late Katian (Boda isotopic event). For most of the Katian and Hirnantian, tropical waters were no farther south than 10°S and the intertropical convergence zone was no farther south than latitude 2°N, well north of the studied sections in Tennessee and Pennsylvania.

***Paleoatmospheric $CO_2$.*** The paleosol paleobarometer of Cerling (1991) estimates past atmospheric $CO_2$ ($P_a$ [ppmv]) from the balance within soils at the depth of carbonate nodules between isotopically light soil $CO_2$ ($\delta^{13}C_s$) compared with isotopically heavy atmospheric $CO_2$ ($\delta^{13}C_a$), and it has been refined for paleoproductivity effects (Breecker and Retallack 2014). A variety of terms in the governing equation (10) below are derived from other analyses and transfer functions. The isotopic composition of soil $CO_2$ ($\delta^{13}C_s$) comes from that of pedogenic carbonate ($\delta^{13}C_c$) using temperature-dependent ($T$ [°C]) fractionation from equation (11) ($R^2 = 0.93$; SE, 0.28‰; Romanek et al. 1992). The isotopic composition of associated soil organic matter ($\delta^{13}C_o$) is used as a proxy for respired soil $CO_2$ ($\delta^{13}C_r$) as well as to calculate the isotopic composition of atmospheric $CO_2$ ($\delta^{13}C_a$) following equation (12) ($R^2 = 0.96$; SE, 1.73‰), derived from data on modern bryophytes (Fletcher et al. 2005). Finally, partial pressure of respired $CO_2$ in soil ($P_r$) is derived from its known relationship with depth to carbonate nodules ($D_o$, corrected for compaction in paleosols using eq. [1] in modern soils expressed in eq. [6]). Some of this respired $CO_2$ in desert soils studied by Cerling (1991) is from root respiration, but much of it in soil pores beyond the rhizosphere is from microbial respiration (Monger et al. 1991), allowing use of these proxies for pre-Devonian paleosols.

$$P_a = P_r \frac{\delta^{13}C_s - 1.0044\delta^{13}C_r - 4.4}{\delta^{13}C_a - \delta^{13}C_s}, \quad (10)$$

$$\delta^{13}C_s = \frac{\delta^{13}C_c + 1000}{[(11.98 - 0.12T)/1000] + 1} - 1000, \quad (11)$$

$$\partial^{13}C_a = 0.665\partial^{13}C_o + 6.128. \quad (12)$$

Analytical data for this calculation are available only for the Potters Mills paleosol, considered coeval with Hirnantian glaciation in Saharan Africa (fig. 3). The isotopic composition of calcite ($\delta^{13}C_c$) in that paleosol is –5.82‰, and coexisting organic matter ($\delta^{13}C_o$) is –21.5‰, both versus PDB standard (Retallack 1993), which falls within the $\Delta^{13}C$ range (carbonate-organic) of –14‰ to –17‰ accepted by Cotton and Sheldon (2012) as well-preserved organic matter. This isotopic value for organic matter is higher than other Ordovician analyses of Tomescu et al. (2009), who present no Hirnantian values. Marine Hirnantian carbonate carbon isotopic values ($\delta^{13}C_c$) are also up to 6‰ higher than before or afterward (HICE of Young et al. 2010; Ghienne et al. 2014). Paleotemperature and productivity estimates for the Potters Mills paleosol are as given in previous paragraphs. SEs of estimates of atmospheric $CO_2$ using equation (10) were calculated by Gaussian error propagation of the five-component SEs (following Breecker and Retallack 2014). Atmospheric $CO_2$ levels calculated using these equations and paleotemperature of 10.9°C (from eq. [9]) for the type Potters Mills clay paleosol is 166 ± 80 ppmv, roughly equal to Pleistocene glacial levels of 180 ppmv (Stocker et al. 2013).

This $CO_2$ estimate of 166 ± 80 is much lower than 4035 ppmv from mass balance modeling in 10-m.yr. steps (Berner 2006)—too long to incorporate the known isotopic volatility of the Hirnantian (LaPorte et al. 2009; Ghienne et al. 2014), which lasted only 1.4 m.yr. (Gradstein et al. 2012). This estimate is also much lower than 2000 ppm, which is a minimum $CO_2$ concentration associated with the "big five" mass extinctions (Retallack 2013*b*). This estimate is also below 3000 ppm (2240–3920 ppm), which Royer (2006) considers the upper limit of $CO_2$ permitting glaciation in a computer-modeled Hirnantian world of lower solar luminosity and no land plants. This latter assumption is doubtful considering evidence for life in Late Ordovician paleosols presented here (fig. 7).

Estimated paleoatmospheric $CO_2$ from the Hirnantian Potters Mills clay paleosol is also lower than

a previous estimate of 4670-ppmv atmospheric $CO_2$ by Yapp and Poths (1992, 1993) for a lateritic paleosol in the Neda Formation in Wisconsin. The age of this paleosol is latest Katian considering marine fauna in underlying rocks (Royer 2006) and carbon isotope stratigraphy of overlying limestones (McLaughlin et al. 2013). The new low atmospheric $CO_2$ estimate for the Potters Mills clay is compatible with Hirnantian continental glaciation in Saharan Africa (Le Heron and Craig 2008), and the greenhouse crisis estimate of Yapp and Poths (1992, 1993) is compatible with a negative carbon isotope anomaly before Hirnantian glaciation (Armstrong et al. 2009*b*; Young et al. 2010). This negative anomaly was also at a time of marine mass extinction (Fan et al. 2009; Harper et al. 2014). The conundrum of continental glaciation at a time of high atmospheric $CO_2$ (LaPorte et al. 2009) is avoided by this new evidence of short-term paleoatmospheric volatility (fig. 12).

## Conclusions

***Paleosol Records.*** Paleosol records of atmospheric changes with high temporal resolution are used here to disentangle conflicting indications of the two main issues of this study: Late Ordovician glaciation and mass extinction. Ordovician paleosols have been challenged (Davies et al. 2010), but field and petrographic features of ancient soils are documented here: clear pedofabric down from erosional surfaces (fig. 2*A*–2*C*), including clay skins (fig. 8*C*, 8*E*), sepic plasmic fabric (fig. 8*E*), and replacive micrite (figs. 7*C*, 8*C*). Ordovician paleosols also have isotopically depleted carbonate for both $\delta^{13}C$ and $\delta^{13}C$, with tight correlation between stable isotopic values characteristic of soils and paleosols (fig. 10). Finally, geochemical mass balance reveals that they collapsed and lost nutrient cations like soils and Miocene paleosols (fig. 9) rather than dilating and gaining nutrient cations like sediments and sedimentary rocks (Brimhall et al. 1992). Thus, evidence presented here supports the interpretation of bioturbated calichebearing beds of the Juniata Formation as paleosols (Retallack 1985, 1993, 2000; Retallack and Feakes 1987; Feakes and Retallack 1988; Driese and Foreman 1991, 1992; Davies and Gibling 2010) rather than marine beds (Davies et al. 2010).

Long sequences of paleosols in the Tumblagooda Sandstone, Mount Chandler Sandstone, and Indulkana Shales in aridland outcrops and drill cores of Central and South Australia (Retallack 2009*b*) give high-resolution Ordovician and Silurian records of paleoclimate and paleoproductivity (circles of fig. 12*A*). Patchy outcrops of paleosols in the Juniata and Neda Formations of Pennsylvania, Tennessee, and Wisconsin (Retallack and Feakes 1988; Driese and Foreman 1991, 1992; Yapp and Poths 1992, 1993, 1994) add paleogeographic coverage and are similar as far as they go (squares in fig. 12*A*).

***Hirnantian Glaciation.*** The evolution of early land plants and increased depth and degree of weathering and biomass on land is revealed by plantlike fossils (fig. 7) and thicker Katian paleosols of increased productivity (fig. 12*A*). Furthermore, the pedogenic paleobarometer applied to one particularly well-understood Hirnantian paleosol reveals atmospheric $CO_2$ levels of only $166 \pm 80$ ppmv, well below modeled thresholds for Ordovician glaciation (Royer 2006). Thus, there is direct evidence from paleosols for drawdown of atmospheric $CO_2$ by increasingly deep and profound chemical weathering and biomass accumulation by Late Ordovician nonvascular land plants (Retallack 2000, 2003; Lenton et al. 2012).

The Ordovician and Silurian paleosol record also has temporal resolution adequate to show short-term volatility in paleoclimate and paleoproductivity on land (fig. 12*A*). A lateritic late Katian paleosol from Wisconsin is direct evidence of 4670-ppmv atmospheric $CO_2$ (Yapp and Poths 1992, 1993), which is considered a very short-lived greenhouse spike, now correlated (following McLaughlin et al. 2013) with the Boda carbon isotopic shift (Armstrong et al. 2009*a*) and deep-calcic paleosols of the latest Katian (Retallack 2009*b*). This is the reason why carbon cycle modeling in 10-m.yr. steps revealed 4035-ppmv $CO_2$ during the Late Ordovician (Berner 2006), as this greenhouse spike and lower $CO_2$ levels of the Hirnantian glaciation lasted less than 1.4 m.yr. (Gradstein et al. 2012).

Hirnantian glaciation has also been linked with increased silicate weathering from Taconic mountain uplift (Kump et al. 1999) and with amalgamating and expanded microcontinents (Saltzman and Young 2004). The mountainous source for the Juniata Formation persisted through to the early Devonian as source for the Shawangunk and Bloomsburg Formations (fig. 1*C*), which lack any evidence of glaciation (Retallack 1985; King 1998; Driese and Mora 2001). The 10-m.yr. trough in marine carbonate $^{87}Sr/^{86}Sr$ (fig. 12*C*) marks lower riverine input relative to marine hydrothermal activity during the Katian and has been linked to decreased weathering at a time of active volcanism (Shields et al. 2003). Coming at a time of increased soil thickness and soil respiration (fig. 12*A*), this lower fluvial contribution to marine carbonate $^{87}Sr/^{86}Sr$ may reflect not decreased silicate weathering but increased ground cover and water retention by bryophytic mats.

***Late Ordovician Mass Extinction.*** The estimate of 4670-ppmv atmospheric $CO_2$ by Yapp and Poths

(1992, 1993) for a lateritic paleosol in the latest Katian Neda Formation of Wisconsin (McLaughlin et al. 2013) coincides with the main pulse of Late Ordovician marine mass extinction just below the *Normalograptus extraordinarius* graptolite zone forming the base of the Hirnantian, which was followed by a second pulse of extinction in the late Hirnantian lower *Normalograptus persculptus* zone (Harper et al. 2014). These extinction levels are also spikes in depth to paleosol carbonate and inferred productivity (fig. 12*A*) and spikes in weathering inferred from marine carbonate $^{87}Sr/^{86}Sr$ (fig. 12*C*). Both pulses of extinction were most severe in high-latitude Gondwanan terranes but were less marked in the tropics (Harper et al. 2014) and not yet detectable in the record of early land plant spores (Steemans et al. 2010; Edwards et al. 2014). The extinction levels are both at abrupt negative carbon isotopic excursions (productivity crises) and positive oxygen isotopic excursions (warming events) in marine carbonate flanking a ca. 1-m.yr. positive excursion (HICE of Armstrong et al. 2009*a*; Young et al. 2010). Comparable spike-like perturbations are also known for a succession of Permian and Triassic extinctions, which rise to the level of mass extinction when inferred atmospheric $CO_2$ from paleosol and *Ginkgo* paleobarometers is more than 2000 ppmv (Retallack et al. 2011; Retallack 2013*b*). Abrupt negative carbon isotopic excursions have been explained by atmospheric pollution with massive amounts of isotopically light $CH_4$, which within a decade oxidizes to a transient $CO_2$ greenhouse, raising planetary temperature and precipitation to deepen paleosol carbonate horizons and leave isotopic signatures in both organic matter and carbonate of paleosols (Retallack et al. 2011*b*; Retallack 2013*b*). The source of such large injections of isotopically light carbon into the atmosphere may have been thermogenic cracking of coal or other organic matter around the feeder dikes of flood basalts (Retallack and Jahren 2008). The Katian negative carbon isotopic excursion stimulated Lefebvre et al. (2010) to postulate a Late Ordovician flood basalt, and this prediction may be represented by widespread tholeiites in the late Katian Yerba Loca and Alcaparrosa Formations of the Cuyana Terrane of the Argentine Precordillera (Ortega et al. 2008; González-Menéndez et al. 2013). Thus, Late Ordovician mass extinction as a preplay of the Late Permian extinction by atmospheric pollution of flood basalt eruptions remains a viable hypothesis.

Alternative hypotheses of Late Ordovician mass extinction include Hirnantian cooling (Harper et al. 2014), but the first wave of the extinction occurs before glacial onset indicated by positive marine carbon isotopic values and glacial facies correlations (Ghienne et al. 2014), and the second wave of extinction occurs during waning phases of glaciation (Armstrong et al. 2009*a*; Young et al. 2010). Many mass extinctions were at times of abrupt global warming, not cooling (Keller 2011; Retallack 2013*b*; Bond and Wignall 2014). Another plausible culprit for Late Ordovician mass extinction is oceanic anoxia (Harper et al. 2014), indicated by black shales with reduced iron, high molybdenum, abundant pyrite framboids, and low sulfide sulfur isotopic values (Armstrong et al. 2009*a*; Fan et al. 2009). These black shales postdate the mass extinction and coincide with the positive marine carbon isotopic excursion (HICE of Armstrong et al. 2009*a*; Young et al. 2010). The delayed onset of Hirnantian euxinia is evidence that oceanic anoxia was a consequence of $CO_2$ greenhouse spikes rather than a first cause of mass extinctions (Retallack 2013*b*). There is no clear evidence of Hirnantian extraterrestrial impact as an extinction method, even in sections in which it has been sought (Wang et al. 1993). A swarm of meteorites is known from the latest Dapingian (Middle Ordovician) limestones in Sweden but is not associated with mass extinction (Schmitz et al. 2008).

## ACKNOWLEDGMENTS

R. Beerbower first suggested the Potters Mills outcrops as potential paleosols, and C. Feakes helped with laboratory studies to develop their geochemical and petrographic potential. S. Driese helped with data and provided a guided tour of the Beans Gap paleosol. I thank D. Breecker, L. Nordt, M. Droser, and D. Bottjer for useful discussions.

## REFERENCES CITED

Aiello, I. W.; Garrison, R. E.; Moore, E. C.; Kastner, M.; and Stakes, D. S. 2001. Anatomy and origin of carbonate structures in a Miocene cold-seep field. Geology 29:1111–1114.

Alvarez, W.; Claeys, P.; and Kieffer, S. W. 1995. Emplacement of Cretaceous-Tertiary boundary shocked quartz from Chicxulub crater. Science 269:930–935.

Arbey, F., and Koeniguer, J.-C. 1979. Les nématophyes et les algueraies de l'Ordovicien et du Dévonien Saharien. Bull. Centr. Rech. Explor. Produc. Elf Aquitaine 3:409–418.

Argast, S. 1992. Enigmatic tubes in Ordovician limestones of the Mohawk Valley, New York. Palaios 7: 532–539.

Armstrong, H. A.; Abbott, G. D.; Turner, B. R; Makhlouf, I. M.; Muhammad, A. B.; Pedentchouk, N.; and Peters, H. 2009*a*. Black shale deposition in an Upper Ordovician-Silurian permanently stratified periglacial basin, southern Jordan. Palaeogeogr. Palaeoclimatol. Palaeoecol. 273: 368–377.

Armstrong, H. A.; Baldini, J.; Challands, T. J.; Gröcke, D. R.; and Owen, A. W. 2009*b*. Response of the Inter-Tropical Convergence Zone to Southern Hemisphere cooling during Upper Ordovician glaciation. Palaeogeogr. Palaeoclimatol. Palaeoecol. 284:227–236.

Australian Bureau of Meteorology. 2015. Climate statistics for Australian stations. Accessed January 27, 2015. http://www.bom.gov.au/.

Barbour, M. M., and Farquhar, G. D. 2000. Relative humidity- and ABA-induced variation in carbon and oxygen isotope ratios of cotton leaves. Plant Cell Environ. 23:473–485.

Barbour, M. M.; Walcroft, A. S.; and Farquhar, G. D. 2002. Seasonal variation in $\delta^{13}C$ and $\delta^{18}O$ of cellulose from growth rings of Pinus radiate. Plant Cell Environ. 25:1483–1499.

Becker, L.; Poreda, R. J.; Basu, A. R.; Pope, K. O.; Harrison, T. M.; Nicholson, C.; and Iasky, R. 2004. Bedout: a possible end-Permian impact crater offshore of northwestern Australia. Science 304:1469–1476.

Belnap, J.; Büdel, B.; and Lange, O. L. 2003. Biological soil crusts: characteristics and distribution. *In* Belnap, J., and Lange, O. L., eds. Biological soil crusts: structure, function and management. Berlin, Springer, p. 177–191.

Berner, R. A. 1997. The rise of plants and their effect on weathering and atmospheric $CO_2$. Science 276: 544–545.

———. 2006. GEOCARBSULF: a combined model for Phanerozoic atmospheric $O_2$ and $CO_2$. Geochim. Cosmochim. Acta 70:5653–5664.

Bond, D. P. G., and Wignall, P. B. 2014. Large igneous provinces and mass extinctions: an update. *In* Keller, G., and Kerr, A. C., eds. Volcanism, impacts, and mass extinctions: causes and effects. Geol. Soc. Am. Spec. Pap. 505:29–55.

Boyce, C. K.; Hotton, C. L.; Fogel, M. L.; Cody, G. D.; Hazen, R. M.; Knoll, A. H.; and Hueber, F. M. 2007. Devonian landscape heterogeneity recorded by a giant fungus. Geology 35:399–402.

Breecker, D. O., and Retallack, G. J. 2014. Refining the pedogenic carbonate atmospheric $CO_2$ proxy and application to Miocene $CO_2$. Palaeogeogr. Palaeoclimatol. Palaeoecol. 406:1–8.

Brenchley, P. J.; Carden, G. A. F.; and Marshall, J. D. 1995. Environmental changes associated with the "first strike" of the Late Ordovician mass extinction. Mod. Geol. 20:69–82.

Brimhall, G. H.; Chadwick, O. A.; Lewis, C. J.; Compston, W.; Williams, I. S.; Danti, K. J.; Dietrich, W. E.; Power, M. E.; Hendricks, D.; and Bratt, J. 1992. Deformational mass transport and invasive processes in soil evolution. Science 255:695–702.

Budd, G. E.; Hogstrom, A. E. S.; and Gogin, I. 2001. A myriapod-like arthropod from the Upper Cambrian of East Siberia. Palaeontol. Z. 75:37–41.

Buggisch, W.; Joachimski, M. M.; Lehnert, O.; Bergström, S. M.; Repetski, J. E.; and Webers, G. F. 2010. Did intense volcanism trigger the first Late Ordovician icehouse? Geology 38:327–330.

Butts, C. 1940. Geology of the Appalachian Valley in Virginia. Va. Geol. Surv. Bull. 52:1–568.

Cerling, T. E. 1991. Carbon dioxide in the atmosphere: evidence from Cenozoic and Mesozoic paleosols. Am. J. Sci. 291:377–400.

Chadwick, O. A., and Chorover, J. 2001. The chemistry of pedogenic thresholds. Geoderma 100:321–353.

Cleal, C. J., and Thomas, B. A. 1995. Palaeozoic palaeobotany of Great Britain. London, Chapman & Hall, 295 p.

Cotter, E. 1978. The evolution of fluvial style, with special reference to the central Appalachian Palaeozoic. *In* Miall, A. D., ed. Fluvial sedimentology. Can. Soc. Petrol. Geol. Mem. 5:361–383.

———. 1983. Shelf, paralic, and fluvial environments and eustatic sea-level fluctuations in the origin of the Tuscarora Formation (Lower Silurian) of central Pennsylvania. J. Sediment. Petrol. 53:25–49.

Cotton, J., and Sheldon, N. D. 2012. New constraints on using paleosols to reconstruct atmospheric $pCO_2$. Geol. Soc. Am. Bull. 124:1411–1423.

Crowell, J. C. 1978. Gondwanan glaciation, cyclothems, continental positioning and climate change. Am. J. Sci. 278:1345–1372.

Davies, N. S., and Gibling, M. R. 2010. Cambrian to Devonian evolution of alluvial systems: the sedimentological impact of the earliest land plants. Earth Sci. Rev. 98:171–200.

Davies, N. S.; Gibling, M. R.; and Rygel, M. C. 2011. Alluvial facies evolution during the Palaeozoic greening of the continents: case studies, conceptual models and modern analogues. Sedimentology 58:220–258.

Davies, N. S.; Rygel, M. C.; and Gibling, M. B. 2010. Marine influence in the Upper Ordovician Juniata Formation (Potters Mills, Pennsylvania): implications for the history of life on land. Palaios 25:527–539.

Dennison, J. M. 1976. Appalachian Queenston Delta related to eustatic sea-level drop accompanying Late Ordovician glaciation centred in Africa. *In* Bassett, M. G., ed. The Ordovician System. Cardiff, University of Wales Press, p. 107–120.

Diecchio, R. J. 1995. Sea-level changes and correlation of Ordovician-Silurian boundary sections in Appalachian Basin and Anticosti Island based on cumulative aggradation plots. *In* Cooper, J. D.; Droser, M. L.; and Finney S. C., eds. Ordovician odyssey: short papers for the Seventh International Symposium on the Ordovician System. Soc. Econ. Paleont. Mineral. Pac. Sect. Los Angeles Field Trip Guidebook 77:337–341.

Diecchio, R. J., and Broderson, B. T. 1994. Recognition of regional (eustatic?) and local (tectonic?) relative sea level events in outcrop and gamma-ray logs, Ordovician, West Virginia. *In* Dennison, J. M., and Ettensohn, F. R., eds. Tectonic and eustatic controls on sedimentary cycles. Soc. Sediment. Geol. Concepts Sediment. Paleontol. 4:171–180.

Diecchio, R. J., and Hall, J. C. 1998. New? trace fossils from the Ordovician-Silurian clastic sequence of West Virginia and Maryland. Geol. Soc. Am. Abstr. 30:10.

Dorsch, J.; Bambach, R. K.; and Driese, S. G. 1994. Basin-rebound origin for the "Tuscarora unconformity" in southwestern Virginia and its bearing on the nature of the Taconic Orogeny. Am. J. Sci. 294:237–255.

Dott, R. H. 2003. The importance of eolian abrasion in supermature quartz sandstones and the paradox of weathering on vegetation-free landscapes. J. Geol. 111:387–405.

Driese, S. G., and Foreman, J. L. 1991. Traces and related chemical changes in a Late Ordovician paleosol, Glossifungites ichnofacies, Southern Appalachians, USA. Ichnos 1:207–219.

———. 1992. Paleopedology and paleoclimatic implications of Late Ordovician vertic paleosols, Juniata Formation, Southern Appalachians. J. Sediment. Petrol. 62:71–83.

Driese, S. G., and Mora, C. I. 2001. Diversification of Siluro-Devonian plant traces in paleosols and influence on estimates of paleoatmospheric $CO_2$ levels. *In* Gensel, P. G., and Edwards, D., eds. Plants invade the land: evolutionary and environmental perspectives. New York, Columbia University Press, p. 237–253.

Driese, S. G.; Simpson, E. L.; and Eriksson, K. A. 1995. Redoximorphic paleosols in alluvial and lacustrine deposits, 1.8 Ga Lochness Formation, Mount Isa, Australia: pedogenic processes and implications for paleoclimate. J. Sediment. Res. A65:675–689.

Drummond, C. N.; Patterson, W. P.; and Walker, J. C. G. 1995. Climatic forcing of carbon-oxygen isotopic covariance in temperate-region marl lakes. Geology 23:1031–1034.

Edwards, D.; Morris, J. L.; Richardson, J. B.; and Kenrick, P. 2014. Cryptospores and cryptophytes reveal hidden diversity in early land floras. New Phytol. 202:50–78.

Ehleringer, J. R., and Cook, C. S. 1998. Carbon and oxygen isotope ratios of ecosystem respiration along an Oregon conifer transect: preliminary observations based on small-flask sampling. Tree Physiol. 18:513–519.

Ehleringer, J. R.; Buchmann, N.; and Flanagan, L. B. 2000. Carbon isotope ratios in belowground carbon cycle processes. Ecol. Appl. 10:412–422.

Epstein, A. G.; Epstein, J. B.; and Harris, C. D. 1977. Conodont colour alteration—an index to organic metamorphism. U.S. Geol. Surv. Prof. Pap. 995:1–27.

Fan, J.-X.; Peng P.-G.; and Melchin, M. J. 2009. Carbon isotopes and event stratigraphy near the Ordovician-Silurian boundary, Yichang, south China. Palaeogeogr. Palaeoclimatol. Palaeoecol. 276:160–169.

Feakes, C. R.; Holland, H. D.; and Zbinden, E. A. 1989. Ordovician paleosols at Arisaig, Nova Scotia, and the evolution of the atmosphere. Catena Suppl. 16:207–232.

Feakes, C. R., and Retallack, G. J. 1988. Recognition and chemical characterization of fossil soils developed on alluvium: a Late Ordovician example. *In* Reinhardt, J., and Sigleo, W. R., eds. Paleosols and weathering through geologic time: principles and applications. Geol. Soc. Am. Spec. Pap. 216:35–48.

Fedo, C. M.; Nesboitt, H. W.; and Young, G. M. 1995. Unraveling the effects of potassium metasomatism in sedimentary rocks and paleosols, with implications for paleoweathering conditions and provenance. Geology 23:921–924.

Finnegan, S.; Bergmann, K.; Eiler, J. M.; Jones, D. S.; Fike, D. A.; Eisenman, I.; Hughes, N. C.; Tripati, A. K.; and Fischer, W. W. 2011. The magnitude and duration of Late Ordovician–Early Silurian glaciation. Science 331:903–906.

Fleming, P. J. G., and Rigby, J. K. 1972. Possible land plants from the Middle Cambrian, Queensland. Nature 238:266.

Fletcher, B. J.; Beerling, D. J.; Brentnall, S. J.; and Royer, D. L. 2005. Fossil bryophytes as recorders of ancient $CO_2$ levels: experimental evidence and a Cretaceous case study. Glob. Biogeochem. Cycles 19:GB3012. doi:10.1029/2005GB002495.

Food and Agriculture Organization. 1974. Soil map of the world. Volume I, legend. Paris, United Nations Educational Scientific and Cultural Organization, 59 p.

Fritsch, A. 1908. Problematica silurica. *In* Barrande, J., ed. Systême silurien du centre de la Bohême. Leipzig, Raimund Gerhard, 28 p.

Gallagher, T. M., and Sheldon, N. D. 2013. A new paleothermometer for forest paleosols and its implications for Cenozoic climates. Geology 41:647–650.

Ghienne, J.-F.; Desrochers, A.; Vandenbroucke, T. R. A.; Achab, A.; Asselin, E.; Dabard, M.-P.; Farley, C.; Loi, A.; Paris, F.; Wickson, S.; and Veizer, J. 2014. A Cenozoic-style scenario for the end-Ordovician glaciation. Nat. Commun. 5489:1–9. doi:10.1038/ncomms5485.

González-Menéndez, L.; Gallastegui, G.; Cuesta, A.; Heredia, N.; and Rubio-Ordoñez, A. 2013. Petrogenesis of Early Paleozoic basalts and gabbros in the western Cuyana terrane: constraints on the tectonic setting of the southwestern Gondwana margin (Sierra del Tigre, Andean Argentine Precordillera). Gondwana Res. 24: 359–376.

Gradstein, F. M.; Ogg, J. G.; Schmitz, M. D.; and Ogg, G. M. 2012. The geologic time scale 2012. Amsterdam, Elsevier, 1144 p.

Graham, L. E.; Cook, M. E.; Hanson, D. T.; Pigg, K. B.; and Graham, J. M. 2010. Structural, physiological isotopic evidence that the enigmatic Paleozoic fossil *Prototaxites* formed from rolled liverwort mats. Am. J. Bot. 97:268–275.

Grandstaff, D. E.; Edelman, M. J.; Foster, R. W.; Zbinden, E.; and Kimberley, M. M. 1986. Chemistry and mineralogy of Precambrian palaeosols at the base of the Dominion and Pongola Groups (Transvaal, South Africa). Precambrian Res. 32:97–131.

Gray, M. B., and Nickelsen, R. P. 1989. Pedogenic slickensides, indicators of strain and deformation processes in redbed sequences of the Appalachian foreland. Geology 17:72–75.

Grice, G.; Cao, C.; Love, G. D.; Böttcher, M. E.; Twitchett, R. J.; Grosjean, E.; Summons, R. E.; Turgeon, S. C.;

Dunning, W.; and Jin, Y. 2005. Photic zone euxinia during the Permian-Triassic superanoxic event. Science 307:706–709.

Hammarlund, E. U.; Dahl, T. W.; Harper, D. A. T.; Bond, D. P. G.; Nielsen, A. T.; Schovsbo, N. H.; Schönlaub, H.-P.; Bjerrum, C. J.; Zalasiewicz, J. A.; and Canfield, D. E. 2012. A sulfidic driver for the end-Ordovician mass extinction. Earth Planet. Sci. Lett. 331–332:128–139.

Harper, D. A. T.; Hammarlund, E. U.; and Rasmussen, C. M. Ø. 2014. End Ordovician extinctions: a coincidence of causes. Gondwana Res. 25:1294–1307.

Hatcher, R. D.; Thomas, W. A.; and Viele, G. W., eds. 1989. The Appalachian-Ouachita Orogen in the United States. Boulder, CO, Geological Society of America, 787 p.

Holland, S. M., and Patzkowsky, M. E. 1998. Sequence stratigraphy and relative sea-level history of the Middle and Upper Ordovician of the Nashville Dome, Tennessee. J. Sediment. Res. 68:684–699.

Horowitz, D. H. 1965. Petrology of the Upper Ordovician and Lower Silurian rocks in the central Appalachians. PhD dissertation, Pennsylvania State University, State College.

Hou, X., and Bergström, J. 1998. Three additional arthropods from the early Cambrian Chengjiang fauna, Yunnan, southwest China. Acta Palaeontol. Sinica 37:395–401.

Huang, C.-M.; Wang, C.-S.; and Tang, Y. 2005. Stable carbon and oxygen isotopes of pedogenic carbonates in Ustic Vertisols: implications for paleoenvironmental change. Pedosphere 15:539–544.

Hueber, F. M. 2001. Rotted wood-alga-fungus: the history and life of Prototaxites Dawson 1859. Rev. Palaeobot. Palynol. 116:123–158.

Isbell, R. F. 1998. The Australian soil classification. Collingwood, CSIRO, 144 p.

Johnson, E. W.; Briggs, D. E. G.; Suthren, R. J.; Wright, J. L.; and Tunnikoff, S. P. 1994. Non-marine arthropod traces from the subaerial Ordovician Borrowdale Volcanic Group, English Lake District. Geol. Mag. 131: 395–406.

Johnson, N. G. 1985. Early Silurian playnomorphs from the Tuscarora Formation of central Pennsylvania and their paleobotanical and geological significance. Rev. Paleobot. Palynol. 45:307–360.

Jutras, P.; Quillan, R. S.; and LeForte, M. J. 2009. Evidence from Middle Ordovician paleosols for the predominance of alkaline groundwater at the dawn of land plant radiation. Geology 37:91–94.

Kasting, J. F.; Howard, T.; Wallmann, K.; Veizer, J.; Shields, G.; and Jaffrés, J. 2006. Paleoclimates, ocean depth, and the oxygen isotopic composition of seawater. Earth Planet. Sci. Lett. 252:82–93.

Keller, G. 2011. The Cretaceous-Tertiary mass extinction theories and controversies. *In* Keller, G., and Adatte, T., eds. The End-Cretaceous mass extinction and the Chicxulub impact in Texas. Soc. Econ. Paleontol. Mineral. Spec. Publ. 100:7–22.

Kennett, J. P. 1982. Marine geology. New York, Prentice-Hall, 813 p.

Kenrick, P.; Wellman C. H.; Schneider, H.; and Edgecombe, G. 2012. A timeline for terrestrialization: consequences for the carbon cycle in the Palaeozoic. Phil. Trans. R. Soc. 367:519–536.

King, D. C. 1998. Interpretation of stable isotope compositions of pedogenic carbonate in Late Silurian to Late Devonian paleosols, Appalachian Basin. MS thesis, University of Tennessee, Knoxville.

Knauth, L. P.; Brilli, M.; and Klonowski, S. 2003. Isotope geochemistry of caliche developed on basalt. Geochim. Cosmochim. Acta 67:185–195.

Kříž, J., and Pojeta, J. 1974. Barrande's colonies concept and a comparison of his stratigraphy with the modern stratigraphy of the middle Bohemian Lower Palaeozoic rocks (Barrandian) of Czechoslovakia. J. Paleontol. 48: 489–494.

Kump, L. R.; Arthur, M. A.; Patzkowsky, M. E.; Gibbs, M. T.; Pinkus, D. S.; and Sheehan, P. M. 1999. A weathering hypothesis for glaciation at high atmospheric $pCO_2$ during the Late Ordovician. Palaeogeogr. Palaeoclimatol. Palaeoecol. 152:173–187.

Landing, E., and MacGabhann, B. A. 2010. First evidence for Cambrian glaciation provided by sections in Avalonian New Brunswick and Ireland: additional data for Avalon-Gondwana separation by the earliest Paleozoic. Palaeogeogr. Palaeoclimatol. Palaeoecol. 285:174–185.

LaPorte, D. F.; Holmden, C.; Patterson, W. P.; Loxton, J. D.; Melchin, M. J.; Mitchell, C. E.; Finney, S. C.; and Sheets, H. D. 2009. Local and global perspectives on carbon and nitrogen cycling during the Hirnantian glaciation. Palaeogeogr. Palaeoclimatol. Palaeoecol. 276:182–195.

Lefebvre, V.; Servais, T.; François, L.; and Averbuch, O. 2010. Did a Katian large igneous province trigger the Late Ordovician glaciation? a hypothesis tested with a carbon cycle model. Palaeogeogr. Palaeoclimatol. Palaeoecol. 296:310–319.

Le Heron, D. P., and Craig, J. 2008. First-order reconstruction of a Late Ordovician Saharan ice sheet. J. Geol. Soc. Lond. 165:19–29.

Lenton, T. M.; Crouch, M.; Johnson, M.; Pires, N.; and Dolan, L. 2012. First plants cooled the Ordovician. Nat. Geosci. 5:86–89.

Liu, X.; An, W.; Steven, W.; Leavitt, S. W.; Wang, W.; Xu, G.; Zeng, X.; and Qin, D. 2014. Recent strengthening of correlations between tree-ring $\delta^{13}C$ and $\delta^{18}O$ in mesic western China: implications to climatic reconstruction and physiological responses. Glob. Planet. Change 113:23–33.

Lohmann, K. G. 1988. Geochemical patterns of metoeric diagentic systems and their application to studies of paleokarst. *In* James, N. P., and Choquette, P. W., eds. Paleokarst. Berlin, Springer, p. 59–80.

Ludvigson, G. A.; González, L. A.; Fowle, D. A.; Roberts, J. A.; Driese, S. G.; Villareal, M. A.; Smith, J. J.; and Suarez, M. B. 2013. Paleoclimatic applications and modern process studies of pedogenic siderite. *In* Driese, S. G., ed. New frontiers in paleopedology and terrestrial paleoclimatology. Soc. Econ. Paleontol. Mineral. Spec. Pap. 44:79–87.

Mack, G. H.; James, W. C.; and Monger, H. C. 1993. Classification of paleosols. Geol. Soc. Am. Bull. 105: 129–136.

Magallón, S.; Hilu, K. W.; and Quandt, D. 2013. Land plant evolutionary timeline: gene effects are secondary to fossil constratints in relaxed clock estimation of age and substitution rates. Am. J. Bot. 100:556–573.

Manzo, D. J.; Bergström, S. M.; Huff, W. D.; and Kolata, D. R. 2002. New data on the age and distribution of the Early Silurian (Llandoverian) Thorn Hill K-bentonite Complex in the Southern Appalachians. North-Central/ Southeast. Sect. Geol. Soc. Am. Abstr. 34:7.

Matsumoto, E.; Naruoka, T.; and da Silva, E. F. 1997. Concentration of carbon dioxide in regolith air in different tropical geoecosystems of northeast Brazil. Inst. Geosci. Univ. Tsukuba Ann. Rep. 23:11–15.

Maynard, J. B. 1992. Chemistry of modern soils as a guide to Precambrian fossil soils. J. Geol. 100:279–289.

McLaughlin, P. I.; Mikulic, D. G.; and Kluessendorf, J. 2013. Age and correlation of Silurian rocks in Sheboygan, Wisconsin, using integrated stable carbon isotope stratigraphy and facies analysis. Geosci. Wis. 21: 14–38.

McNamara, K. J., and Trewin, N. H. 1993. A euthycarcinoid arthropod from the Silurian of western Australia. Palaeontology 36:319–335.

McWilliams, A. S.; Mutti, L. J.; Mathur, R.; Detrie, T. A.; and Gold, D. P. 2006. New homogenization data for fluid inclusions in fault related quartz veins in the Bald Eagle Fm. in central PA. Geol. Soc. Am. Abstr. 38:79.

Melim, L. A.; Swart, P. K.; and Eberli, G. P. 2004. Mixing zone diagenesis in the subsurface of Florida and the Bahamas. J. Sediment. Res. 76:904–913.

Mikuláš, R. 1995. Trace fossils from the Paseky Shale (early Cambrian, Czech Republic). Czech Geol. Soc. J. 40:37–44.

Misof, B.; Liu, S.; Meusemann, K.; Peters, R. S.; Donath, A.; Mayer, C.; Frandsen, P. B.; et al. 2014. Phylogenomics resolves the timing and pattern of insect evolution. Science 346:763–767.

Monger, H. C.; Daugherty, L. A.; Lindemann, W. C.; and Liddell, C. M. 1991. Microbial precipitation of pedogenic calcite. Geology 19:997–1000.

Neaman, A.; Chorover, J.; and Brantley, S. L. 2005. Implications of the evolution of organic acid moieties for basalt weathering over geological time. Am. J. Sci. 305:147–185.

Nesbitt, H. W., and Young, G. M. 1982. Early Proterozoic climates and plate motions inferred from major element chemistry of lutites. Nature 299:715–717.

Ortega, G.; Albanesi, G. L.; Banchig, A. L.; and Peralta, G. L. 2008. High resolution conondont-graptolite biostratigraphy in the Middle-Upper Ordovician of the Sierra de La Invernada Formation (Central Precordillera, Argentina). Geol. Acta 6:161–180.

Óskarsson, B. V.; Riishuus, M. S.; and Arnalds, O. 2009. Climate-dependent chemical weathering of volcanic soils in Iceland. Geoderma 189–190:635–651.

Osgood, R. G. 1970. Trace fossils of the Cincinnati area. Palaeontol. Am. 6:281–444.

Passchier, S., and Krissek, L. A. 2008. Oligocene-Miocene Antarctic continental weathering record and paleoclimatic implications, Cape Roberts Drilling Project, Ross Sea, Antarctica. Palaeogeogr. Palaeoclimatol. Palaeoecol. 260:30–40.

Paton, T. R. 1974. Origin and terminology for gilgai in Australia. Geoderma 11:221–242.

Paton, T. R.; Humphreys, G. S.; and Mitchell, P. B. 1995. Soils: a new global view. New Haven, CT, Yale University Press, 213 p.

Peckmann, J.; Goedert, J. L.; Thiel, V.; Michaelis, W.; and Reitner, J. 2002. A comprehensive approach to the study of methane-seep deposits from the Lincoln Creek Formation, western Washington State, USA. Sedimentology 49:855–873.

Prokoph, A.; Shields, G. A.; and Veizer, J. 2008. Compilation and time-series analysis of a marine carbonate $\delta^{18}O$, $\delta^{13}C$, $^{87}Sr/^{86}Sr$ and $\delta^{34}S$ database through Earth history. Earth Sci. Rev. 87:113–133.

Raymo, M. E. 1991. Geochemical evidence supporting T. C. Chamberlin's theory of glaciation. Geology 199: 344–347.

Raymo, M. E., and Ruddiman, W. F. 1992. Tectonic forcing of late Cenozoic climate. Nature 359:117–122.

Redecker, D.; Kodner, R.; and Graham, L. E. 2000. Glomalean fungi from the Ordovician. Science 289:1920–1921.

Retallack, G. J. 1985. Fossil soils as grounds for interpreting the advent of large plants and animals on land. Phil. Trans. R. Soc. Lond. B309:105–142.

———. 1991. Miocene paleosols and ape habitats from Pakistan and Kenya. New York, Oxford University Press, 346 p.

———. 1992. What to call early plant formations on land. Palaios 7:508–520.

———. 1993. Late Ordovician paleosols of the Juniata Formation, near Potters Mills, PA. *In* Driese, S. G., ed. Paleosols, paleoclimate and paleoatmospheric $CO_2$: Paleozoic paleosols of central Pennsylvania. Univ. Tenn. Dep. Geol. Sci. Stud. Geol. 22:33–50.

———. 1997. Paleosols in the upper Narrabeen Group of New South Wales as evidence of Early Triassic palaeoenvironments without exact modern analogues. Australas. J. Earth Sci. 44:185–201.

———. 1998. Fossil soils and completeness of the rock and fossil record. *In* Donovan, S. K., and Paul, C. R. C., eds. The adequacy of the fossil record. Chichester, Wiley, p. 131–162.

———. 2000. Ordovician life on land and early Paleozoic global change. *In* Gastaldo, R. A., and DiMichele, W. A., eds. Phanerozoic ecosystems. Paleontol. Soc. Pap. 6:21–45.

———. 2001*a*. *Scoyenia* burrows from Ordovician paleosols of the Juniata Formation in Pennsylvania. Palaeontology 44:209–235.

———. 2001*b*. Soils of the past. Oxford, Blackwell, 404 p.

———. 2003. Soils and global change in the carbon cycle over geological time. *In* Holland, H. D., and Turekian, K. K., eds. Treatise on geochemistry (vol. 5). Oxford, Pergamon, p. 581–605.

———. 2004. End-Cretaceous acid rain as a selective extinction mechanism between birds and dinosaurs. *In* Currie, P. J.; Koppelhus, E. B.; Shugar, M. A.; and. Wright, J. L., eds. Feathered dragons: studies on the transition from dinosaurs to birds. Indianapolis, Indiana University Press, p. 35–64.

———. 2005. Pedogenic carbonate proxies for amount and seasonality of precipitation in paleosols. Geology 33:333–336.

———. 2008. Cambrian paleosols and landscapes of South Australia. Australas. J. Earth Sci. 55:1083–1106.

———. 2009*a*. Cambrian-Ordovician non-marine fossils from South Australia. Alcheringa 33:355–391.

———. 2009*b*. Early Palaeozoic pedostratigraphy and global events in Australia. Australas. J. Earth Sci. 56: 569–584.

———. 2009*c*. Refining a pedogenic $CO_2$ palaeobarometer for quantifying the middle Miocene greenhouse spike. Palaeogeogr. Palaeoclimatol. Palaeoecol. 281: 57–65.

———. 2012. Mallee model for mammal communities of the early Cenozoic and Mesozoic. Palaeogeogr. Palaeoclimatol. Palaeoecol. 342–343:111–129.

———. 2013*a*. Global cooling by grasslands in the geological past and near future. Ann. Rev. Earth Planet. Sci. 41:69–86.

———. 2013*b*. Permian and Triassic greenhouse crises. Gondwana Res. 24:90–103.

Retallack, G. J.; Davies, N. S.; Rygel, M. C.; and Gibling, M. R. 2011*a*. Marine influence in the Upper Ordovician Juniata Formation (Potters Mills, Pennsylvania): implications for the history of life on land: comment and reply. Palaios 26:765–769.

Retallack, G. J., and Feakes, C. R. 1987. Trace fossil evidence for Late Ordovician animals on land. Science 235:61–63.

Retallack, G. J., and Huang, C.-M. 2011. Ecology and evolution of Devonian trees in New York, USA. Palaeogeogr. Palaeoclimatol. Palaeoecol. 299:110–128.

Retallack, G. J., and Jahren, A. H. 2008. Methane release from igneous intrusion of coal during Late Permian extinction events. J. Geol. 116:1–20.

Retallack, G. J., and Landing, E. 2014. Affinities and architecture of Devonian trunks of *Prototaxites loganii*. Mycologia 106:1143–1156.

Retallack, G. J.; Marconato, A.; Osterhout, J. T.; Watts, K. E.; and Bindeman, I. N. 2014. Revised Wonoka isotopic anomaly in South Australia and Late Ediacaran mass extinction. J. Geol. Soc. Lond. 171:709–722.

Retallack, G. J.; Seyedolali, A.; Krull, E. S.; Holser, W. T.; Ambers, C. A.; and Kyte, F. T. 1998. Search for evidence of impact at the Permian-Triassic boundary in Antarctica and Australia. Geology 26:979–982.

Retallack, G. J.; Sheldon, N. D.; Carr, P. F.; Fanning, M.; Thompson, C. A.; Williams, M. L.; Jones, B. G.; and Hutton, A. 2011*b*. Multiple Early Triassic greenhouse crises impeded recovery from Late Permian mass extinction. Palaeogeogr. Palaeoclimatol. Palaeoecol. 308: 233–251.

Retallack, G. J.; Sheldon, N. D.; Cogoini, M.; and Elmore, R. D. 2003. Magnetic susceptibility of early Paleozoic and Precambrian paleosols. Palaeogeogr. Palaeoclimatol. Palaeoecol. 198:373–380.

Rickards, R. B. 2000. The age of the earliest clubmosses: the Silurian Baragwanathia flora, Victoria, Australia. Geol. Mag. 137:207–209.

Romanek, C. S.; Grossman, E. L.; and Morse, J. W. 1992. Carbon isotopic fractionation in synthetic aragonite and calcite: effects of temperature and precipitation rate. Geochim. Cosmochim. Acta 56:419–430.

Romell, L. G. 1935. An example of millipedes as mull formers. Ecology 16:67–71.

Rota-Sabelli, O.; Daley, A. C.; and Pisani, D. 2013. Molecular timetrees reveal a Cambrian colonization of land and a new scenario for ecysozoan evolution. Curr. Biol. 23:392–398.

Royer, D. L. 2006. $CO_2$-forced climate thresholds during the Phanerozoic. Geochim. Cosmochim. Acta 70:5665–5675.

Runkel, A. C.; Mackey, T. J.; Cowan, C. A.; and Fox, D. L. 2010. Tropical shoreline ice in the late Cambrian: implications for Earth's climate between the Cambrian Explosion and the Great Ordovician Biodiversification Event. GSA Today 11:4–10.

Saltzman, M. R., and Young, S. A. 2004. Long-lived glaciation in the Late Ordovician? isotopic and sequence-stratigraphic evidence from western Laurentia. Geology 33:109–112.

Schmitz, B.; Harper, D. A. T.; Peuckner-Ehrenbrink, B.; Stouge, S.; Alwmark, C.; Cronholm, A.; Bergström, S. M.; Tassinari, M.; and Wang, X. 2008. Asteroid breakup linked to the Great Ordovician Biodiversification Event. Nat. Geosci. 1:49–53.

Schuchert, C. 1916. Silurian formations of southeastern New York, New Jersey and Pennsylvania. Geol. Soc. Am. Bull. 27:531–554.

Scotese, C. R. 1997. Point Tracker for Windows [computer program]. Arlington, TX, Paleomap Project.

Sephton, M. A.; Jiao, D.; Engel, M. H.; Looy, C. V.; and Visscher, H. 2015. Terrestrial acidification during the end-Permian biosphere crisis? Geology 43:159–162.

Sheehan, P. M., and Schiefelbein, D. R. J. 1984. The trace fossil Thalassinoides from the Upper Ordovician of the Great Basin: deep burrowing in the Palaeozoic. J. Paleontol. 58:440–447.

Sheldon, N. D., and Retallack, G. J. 2001. Equation for compaction of paleosols due to burial. Geology 29:247–250.

Sheldon, N. D.; Retallack, G. J.; and Tanaka, S. 2002. Geochemical climofunctions from North American soils and application to paleosols across the Eocene-Oligocene boundary in Oregon. J. Geol. 110:687–696.

Shelley, R. M., and Golovatch, S. I. 2011. Atlas of myriapod biogeography. I. Indigenous ordinal and supraordinal distributions in the Diplopoda: perspectives on taxon origina and ages, and an hypothesis on the origin and early evolution of the class. Insecta Mundi 158:1–134.

Shields, G. A.; Carden, G. A. F.; Veizer, J. N.; Meidla, T.; Rong, J.-Y.; and Li, R.-U. 2003. Sr, C, and O isotope

geochemistry of Ordovician brachiopods: a major isotopic event around the Middle-Late Ordovician transition. Cosmochim. Geochim. Acta 67:2005–2025.

Soil Survey Staff. 2010. Keys to soil taxonomy. Washington, DC, National Resources Conservation Service, 338 p.

Southgate, P. N. 1986. Cambrian phoscrete profiles, coated grains and microbial processes in phosphogenesis, Georgina Basin, Australia. J. Sediment. Petrol. 56: 429–441.

Stace, H. C. T.; Hubble, G. D.; Brewer, R.; Northcote, K. H.; Sleeman, J. R.; Mulcahy, M. J.; and Hallsworth, E. G. 1968. A handbook of Australian soils. Adelaide, Rellim, 435 p.

Steemans, P.; Wellman, C. H.; and Gerrienne, P. 2010. Palaeogeography and paleoclimatic considerations based on Ordovician to Lochkovian vegetation. *In* Vecoli, M.; Clément, G.; and Meyer-Berthaud, B., eds. The terrestrialization process: modelling complex interactions in the biosphere-geosphere interface. Geol. Soc. Spec. Publ. 339:49–58.

Stocker, T. F.; Qin, D.; Plattner, G.-K.; Tignor, M.; Allen, S. K.; Boschung, J.; Nauels, A.; Xia, Y.; Bex, V.; and Midgley, P. M., eds. 2013. Climate Change 2013: the physical science basis: summary for policymakers. Cambridge, Cambridge University Press, 27 p.

Surge, D. M.; Savarese, M.; Dodd, J. R.; and Lohmann, K. C. 1997. Carbon isotopic evidence for photosynthesis in early Cambrian oceans. Geology 25:503–506.

Talbot, M. R. 1990. A review of the palaeohydrological interpretation of carbon and oxygen isotopic ratios in primary lacustrine carbonates. Chem. Geol. 80: 261–279.

Terry, R. D., and Chilingar, G. V. 1955. Summary of "Concerning some additional aids in studying sedimentary formations" by M. S. Shvetsov. J. Sediment. Petrol. 25:229–234.

Thompson, A. M. 1968. Sedimentologic and geochemical studies of the Bald Eagle–Juniata colour boundary, central Pennsylvania. PhD dissertation, Brown University, Providence, RI, 264 p.

———. 1970*a*. Geochemistry of colour genesis in red-bed sequence, Juniata and Bald Eagle Formations, Pennsylvania. J. Sediment. Petrol. 40:599–615.

———. 1970*b*. Tidal-flat deposition and early dolomitization in Upper Ordovician rocks of southern Appalachian Valley and Ridge. J. Sediment. Petrol. 40:1271–1286.

———. 1999. Ordovician. *In* Shultz, C. H., ed. The geology of Pennsylvania. Harrisburg, PA, Geological Survey of Pennsylvania, p. 75–89.

Tomescu, A. M. F., and Rothwell, G. W. 2006. Wetlands before tracheophytes: thalloid terrestrial communities of the Early Silurian Passage Creek biota (Virginia). *In* Greb, S. F., and DiMichele, W. A., eds. Wetlands through time. Geol. Soc. Am. Spec. Pap. 399:41–56.

Tomescu, A. M. F.; Pratt, L. M.; Rothwell, G. W.; Strother, P. K.; and Nadon, G. C. 2009. Carbon isotopes support the presence of extensive land floras pre-dating the origin of vascular plants. Palaeogeogr. Palaeoclimatol. Palaeoecol. 283:46–59.

Toye, S. A. 1967. Observations on the biology of three species of Nigerian millipedes. J. Zool. 152:67–78.

Trench, A.; McKerrow, W. S.; and Torsvik, T. H. 1991. Ordovician magnetostratigraphy: a correlation of global data. J. Geol. Soc. Lond. 148:949–957.

Trewin, N. H., and McNamara, K. J. 1994. Arthropods invade the land: trace fossils and palaeoenvironments of the Tumblagooda Sandstone (?late Silurian) of Kalbarri, Western Australia. R. Soc. Edinb. Earth Sci. Trans. 85:177–210.

Ufnar, D. F.; Gröcke, D. R.; and Beddows, P. A. 2008. Assessing pedogenic calcite stable-isotope values: can positive linear covariant trends be used to quantify palaeo-evaporation rates? Chem. Geol. 256:46–51.

van Breemen, N.; Mulder, J.; and Driscoll, C. T. 1983. Acidification and alkalization of soils. Plant Soil 75: 283–308.

van de Schootbrugge, B.; Bachan, A.; Suan, G.; Richoz, S.; and Payne, J. L. 2013. Microbes, mud and methane: cause and consequence of recurrent Early Jurassic anoxia following the end-Triassic mass extinction. Palaeontology 56:1–25.

Vecoli, M.; Delabroye, A.; Spina, A.; and Hints, O. 2011. Cryptospore assemblages from Upper Ordovician (Katian-Hirnantian) strata of Anticosti Island, Québec, Canada, and Estonia: palaeophytogeographic and palaeoclimatic implications. Rev. Palaeobot. Palynol. 166:76–93.

Veizer, J.; Ala, D.; Azmy, K.; Bruckschen, P.; Buhl, D.; Bruhn, F.; Carden, G. A. F.; et al. 1999. $^{87}Sr/^{86}Sr$, $\delta^{13}C$ and $\delta^{18}O$ evolution of Phanerozoic seawater. Chem. Geol. 161:59–88.

Wang, K.; Chatterton, B. D. E.; Attrep, M.; and Orth, C. J. 1993. Late Ordovician mass extinction in the Selwyn Basin, northwestern Canada: geochemical, sedimentological and paleontological evidence. Can. J. Earth Sci. 30:1870–1880.

Watanabe, Y.; Stewart, B. W.; and Ohmoto, H. 2004. Organic- and carbonate-rich soil formation approximately 2.6 billion years ago at Schagen, east Transvaal District, South Africa. Geochim. Cosmochim. Acta 68:2129–2151.

Yapp, C. J., and Poths, H. 1992. Ancient atmospheric $CO_2$ pressures inferred from natural goethites. Nature 355:342–344.

———. 1993. The carbon isotope geochemistry of goethite ($\alpha$-FeOOH) in ironstone of the Upper Ordovician Neda Formation, Wisconsin, USA: implications for early Paleozoic continental environments. Geochim. Cosmochim. Acta 57:2599–2611.

———. 1994. Productivity of pre-vascular biota inferred from $Fe(CO_3)OH$ content of goethite. Nature 368: 49–51.

Young, S. A.; Saltzman, M. R.; Ausich, W. J.; Desrochers, A.; and Kaljo, D. 2010. Did changes in atmospheric $CO_2$ coincide with latest Ordovician glacial-interglacial cycles? Palaeogeogr. Palaeoclimatol. Palaeoecol. 296: 376–388.